

Original paper

# Perspectives on premetamorphic stratabound tourmalinites

John F. SLACK

U.S. Geological Survey (Emeritus), National Center, MS 954, Reston, VA 20192 USA; [jfslack@usgs.gov](mailto:jfslack@usgs.gov)  
Department of Earth Sciences, Memorial University of Newfoundland, St. John's, NL A1B 3X5 Canada



Stratabound tourmalinites are metallogenically important rocks that locally show a close spatial association with diverse types of mineralization, especially volcanogenic massive sulfides (VMS) and clastic-dominated (CD) Zn–Pb deposits. These tourmalinite occurrences span the geologic record from Eoarchean to Jurassic. Host lithologies are dominated by clastic metasedimentary rocks but in some areas include metavolcanic rocks, marble, or metaevaporites. Stratabound and stratiform (conformable) tourmalinites commonly display sedimentary structures such as graded beds, cross-beds, and rip-up clasts. In most cases, field and microtextural relationships are consistent with a synsedimentary to early diagenetic introduction of boron as a precursor to tourmaline formation. Whole-rock geochemical data for major, trace, and rare earth elements (REE) provide valuable insights into tourmalinite origins. Al-normalized values relative to those for least-altered host metasedimentary rocks suggest that tourmalinites in proximal settings at or near hydrothermal vent sites characterized by high fluid/rock regimes (e.g., Sullivan Pb–Zn–Ag deposit, Canada) have very different signatures than those in low fluid/rock, distal settings (e.g., Broken Hill Pb–Zn–Ag deposit, Australia). The high fluid/rock regimes at Sullivan show large mass changes of +60 % for Mg and +180 % for Mn, as well as large variations in abundances of light and middle REE. In contrast, tourmalinite formation in low fluid/rock regimes yields minimal Al-normalized changes in major elements, trace elements, and REE. Boron isotope values of tourmalinite-hosted tourmaline vary widely from –26.1 to +27.5 ‰, and are attributed mainly to boron sources (e.g., sediments, evaporites) with generally minor influence from processes such as formational temperature, fluid/rock ratio, and secular variation in seawater  $\delta^{11}\text{B}$  values. Laterally extensive stratiform tourmalinites formed mainly by syngenetic or early diagenetic processes on or beneath the seafloor. The syngenetic process is attributed to the interaction of vented B-rich brines with aluminous minerals in sediments, whereas the diagenetic process involves the selective replacement of aluminous sediments by B-rich fluids. Modern examples of tourmalinites, as yet undiscovered, may exist in metalliferous sediments of the Red Sea and the eastern Pacific Ocean, in altered volcanoclastic sediments within active seafloor-hydrothermal systems of the South Pacific, and in hydrothermal mounds and vents associated with mafic sill complexes in extensional basins as in the North Sea and South China Sea. Stratabound tourmalinites that contain base-metal sulfides, high Mn concentrations (>1 wt. % MnO), or positive Eu anomalies can be valuable exploration guides for base-metal sulfide deposits in sedimentary and volcanic terranes.

*Keywords:* Tourmalinite, Metallogeny, Syngenetic, Diagenetic, Boron Isotopes, Genetic Models  
*Received:* 9 January 2022; *accepted:* 17 July 2022; *handling editor:* H. Marschall

## 1. Introduction

Tourmalinites are defined as rocks that contain more than 15 to 20 vol. % tourmaline (Slack et al. 1984). These distinctive rocks are geologically and metallogenically important in recording fluid flow in sedimentary and volcanic terranes, and occur in spatial associations with a variety of mineral deposits (Slack 1996), especially Cu–Zn–Pb–Ag–Au volcanogenic massive sulfides (VMS) and clastic-dominated (CD) Zn–Pb (formerly sedex) deposits. Stratabound tourmalinites are broadly concordant with host metasedimentary or metavolcanic lithologies and include discordant feeder zones to overlying sulfide deposits. Stratiform varieties represent a more restricted case of a bedded and conformable geometry on outcrop and microscopic scales. Stratiform tourmalinites, typically less than a few meters thick, have locally been

traced along strike for up to several kilometers (Slack et al. 1993).

Syngenetic or diagenetic origins for stratabound and stratiform tourmalinites have been proposed based on many geological, structural, and geochemical studies worldwide (e.g., Slack et al. 1984; Mao 1995; Pesquera and Velasco 1997; Golani et al. 2002; Tourn et al. 2004; Ferla and Meli 2007; Čopjaková et al. 2009; Martínez-Martínez et al. 2010; Yücel-Öztürk et al. 2015; McGloin et al. 2019). However, detailed studies in some areas have clearly documented epigenetic origins involving metamorphic or magmatic processes (e.g., Steven and Moore 1995; Raith et al. 2004; Sengupta et al. 2005; Vial et al. 2007; Yang and Jiang 2012; Pirajno 2013; Mahjoubi et al. 2016; Kalliomäki et al. 2017; Spránitz et al. 2018; Nabelek 2021). Such post-diagenetic tourmalinites are generally, although not uniformly, distinguished by a lack

of lateral continuity (<10 m along strike) and proximity to shear zones and veins or to granitic intrusions. Not discussed here are well-documented metamorphogenic or magmatic-hydrothermal varieties of tourmalinites, the focus instead being on stratabound and stratiform tourmalinites that lack such associations.

This report is an update of Slack (1996) in presenting information on a larger number of tourmalinites as well as revised insights for genetic models and applications to mineral exploration. Included are selected whole-rock geochemical data and a new compilation of boron isotopic values. Also considered are potential modern analogs of tourmalinites and the possible relevance of these chemically distinctive rocks for the evolution of early life on Earth.

## 2. Geological and mineralogical characteristics

### 2.1. Identification and timing

It is important to first emphasize that some tourmalinites can be easily misidentified as compositionally different rock types (Slack et al. 1984). For example, in weakly metamorphosed terranes, very fine-grained tourmalinite may resemble carbonaceous argillite or siltstone as at the Golden Dyke dome in Australia (Nicholson 1980; Plimer 1986), carbonaceous laminae within stromatolites as in the Barberton greenstone belt in South Africa (Byerly and Palmer 1991), or dark chert as in the Belt-Purcell Supergroup in the U.S. and Canada (Slack 1993; Slack et al. 2000b). In highly metamorphosed terranes, coarse-grained tourmalinite has been mistaken for hornblende amphibolite in the Broken Hill district of Australia (Barnes 1988; Slack et al. 1993). Because of potential geological and metallogenic significance, it is therefore critical during field work and related petrographic study that tourmalinites not be overlooked or misidentified, especially stratiform varieties that generally have a premetamorphic origin.

A longstanding problem is the difficulty in constraining the timing of tourmalinite formation relative to local effects of deformation, metamorphism, or granitic magmatism. For example, Steven and Moore (1995) used detailed mapping to demonstrate that stratabound tourmalinites in the Neoproterozoic Damara orogen of central Namibia are mostly discordant to bedding, having formed during deformation and/or metamorphism; however, some are stratiform and thus likely record early boron introduction and tourmalinite formation. In the Orobic Alps of northern Italy, cryptocrystalline tourmalinites occurring along basement-cover décollements are attributed to the boron metasomatic replacement of tectonic cataclasites (Slack et al. 1996; Zanchi et al. 2019).

Other integrated field and laboratory studies, such as in the Betic Cordillera of Spain (Torres-Ruiz et al. 2003), suggest that stratabound tourmalinites distal from granites nevertheless have an origin directly related to felsic magmatism. These examples testify to the importance of detailed examination of the field and textural (including microtextural) relationships, and integration of these results with relevant geochemical data to properly evaluate the timing of tourmalinite formation in deformed and metamorphosed terranes (e.g., Pesquera et al. 2005).

### 2.2. Ages and geologic settings

Table 1 lists geological and metallogenic data for stratabound tourmalinites worldwide. Based on published descriptions, such tourmalinites are considered premetamorphic, although detailed structural and microtextural studies have not been done in all cases to verify this interpretation. Localities are reported from all seven continents, including Antarctica. Ages range from Eoarchean to Jurassic, the former tourmalinites occurring in some of the oldest sedimentary rock sequences known on Earth, in the 3.7 to 3.8 Ga Isua supracrustal belt of West Greenland (Appel 1995). Metamorphic grades of host rocks to the tourmalinites vary widely from sub-greenschist through amphibolite to granulite, the last being uncommon (Slack 1996).

Host lithologies are dominated by siliciclastic metasediments with or without mafic to felsic metavolcanic rocks. Marble and metaevaporites are important in some areas, as are metamorphosed chemical sediments including chert, iron formation, and Mn-rich rocks such as coticule that mainly comprises fine-grained quartz and spessartine garnet (Spry 1990; Spry et al. 2000). Most premetamorphic stratabound tourmalinites spatially associated with base-metal mineralization are related to VMS and CD Zn–Pb deposits (Fig. 1a, 1b); less common are associations with cobalt or tungsten mineralization, or with iron formations. Importantly, many tourmalinites lack known links to metallic mineralization.

Some metasedimentary terranes without base-metal or other types of mineralization contain relatively abundant tourmalinite (Fig. 1b). These terranes include diverse settings such as (1) tourmalinized sediments peripheral to growth faults and along the contacts of sandstone beds; (2) tourmaline-rich interlaminae with siltstone, argillite, and/or chert; (3) tourmalinized sediments near the borders of synsedimentary mafic sills; (4) stratiform units adjacent to or interlayered with coticule beds (Fig. 2a); and (5) tourmalinized breccia bodies a few meters to as much as several hundred meters in diameter, as in the Mesoproterozoic Belt-Purcell Supergroup that are interpreted as tourmalinized mud volcano deposits (Slack et al. 1998; Turner et al. 2000). On a wider scale, coticule-related tourmalinites represent an important association found in numerous early

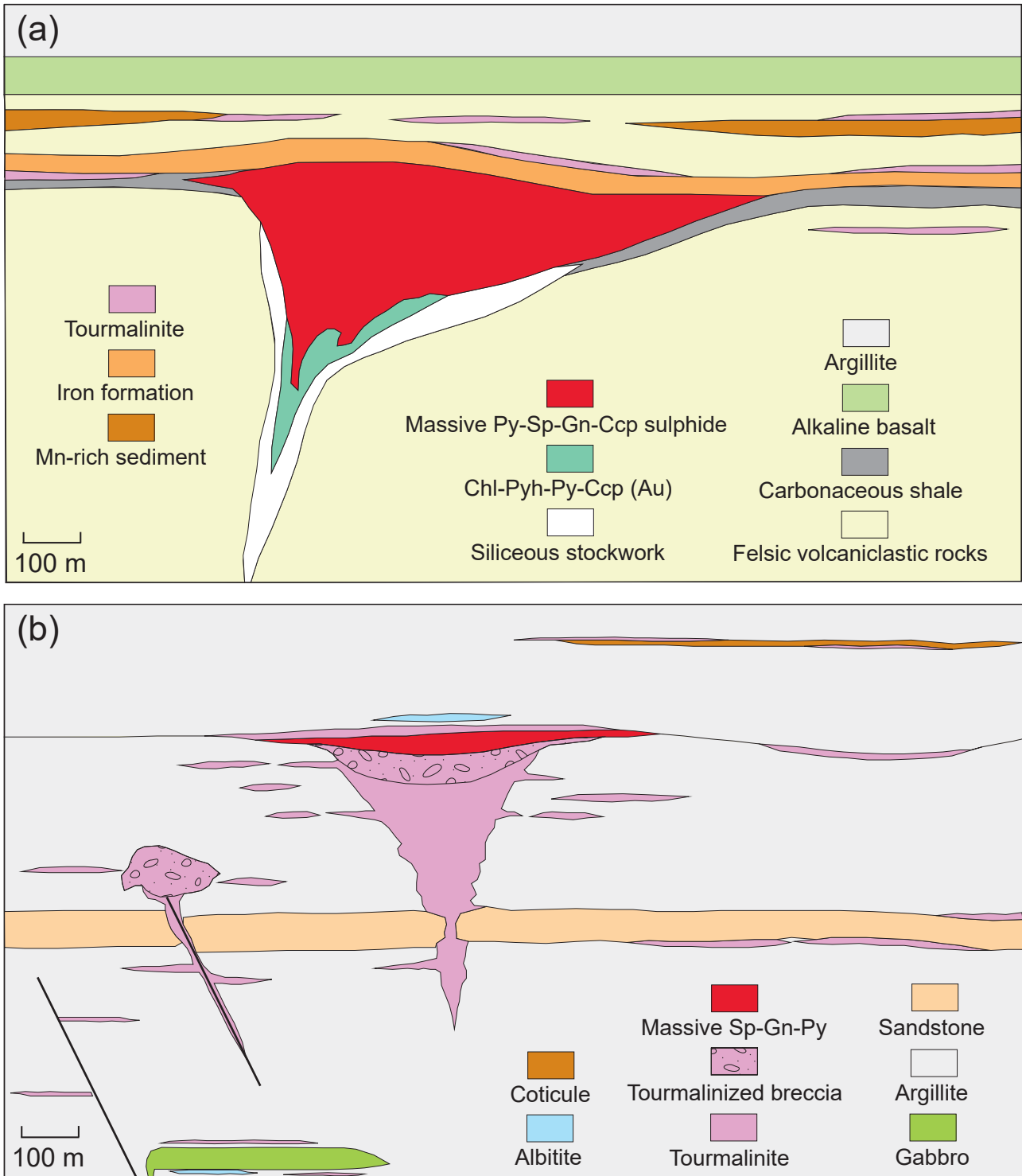


**Fig. 1** Idealized cross-sections showing domains of tourmalinite formation in volcanic- and sediment-hosted stratabound sulfide systems. **a** – Volcanogenic massive sulfide deposits based on felsic-siliciclastic-type settings (modified from Galley et al. 2007). Note the presence of tourmalinites below, above, and peripheral to sulfide zones. **b** – Clastic-dominated Zn–Pb–Ag deposits based on Sullivan-type settings (modified from Slack 1996). Note tourmalinite occurrences in diverse locations, including footwall feeder zones; below, above, and peripheral to sulfide zones; along and marginal to growth faults; and in brecciated (fragmental) sedimentary rocks interpreted as mud-volcano deposits (see Turner et al. 2000). Coticule beds, where present, are typically interlayered with tourmalinite. The thicknesses of some units are exaggerated for clarity. Abbreviations: Ccp, chalcopyrite; Chl, chlorite; Gn, galena; Py, pyrite; Pyh, pyrrhotite; Sp, sphalerite.

Tab. 1 Geological, mineralogical, and metallogenic data for premetamorphic stratabound tourmalinites

Location <sup>1</sup>	Age	Host rocks <sup>2</sup>	Mineral assemblage <sup>3</sup>	Associated mineralization	References <sup>4</sup>
Isua supracrustal belt, West Greenland	Eoarchean	Mvols ± Cmsd ± If	Qz + Tur ± Pyh ± Py ± Ccp	None	1
Barberton greenstone belt, South Africa	Paleoarchean	Mbas + Mumv + Mvcp	Qz + Tur ± Ms ± Py	None	2, 3
Dixon Island Formation, WA, Australia	Mesoarchean	Chert + Mrhy + Cmsd	Qz + Tur ± Ms	None	4
Diverse terranes, West Greenland	Mesoarchean–Neoarchean	Cmsd ± Amph	Qz + Tur ± Ms ± Chl ± Pl ± Ath	Zn ± Cu ± Ag; W	5–9
Cuxiú Formation, Carajas district, northern Brazil	Neoarchean	Cmsd ± Albt	Qz + Tur ± Ab ± Kfs ± Brt ± Phl	Cu ± Au	10
Piriviri Group, northern Zimbabwe	Paleoproterozoic	Cmsd ± Amph	Qz + Tur	W	11
Eastern Senegal–western Mali	Paleoproterozoic	Cmsd ± Mrhy ± Albt ± Marb	Qz + Tur	None	12
Globe Pb–Zn–Ag mine, Broken Hill, NSW, Australia	Paleoproterozoic	Cmsd ± Mrhy ± Albt	Qz + Tur + Ghn + Sps ± Pyh ± Gn ± Mag ± Ms	Pb + Zn + Ag	13
Broken Hill block, NSW, Australia	Paleoproterozoic	Cmsd ± Mrhy	Qz + Tur ± Ab ± Ghn ± Ms ± Sps ± Pyh	Pb + Zn + Ag; W; Co	13–16
Olary block, SA, Australia	Paleoproterozoic	Cmsd ± Csil + If	Qz + Tur + Ab	Co	17, 18
Pegmont, QLD, Australia	Paleoproterozoic	Cmsd ± Amph	Qz + Tur	Pb + Zn + Ag	18, 19
Jervois Range, NT, Australia	Paleoproterozoic	Cmsd ± If ± Cot	Qz + Tur	Pb + Zn + Ag ± Cu	20, 21
Golden Dyke dome, NT, Australia	Paleoproterozoic	Cmsd	Qz + Tur	Au	16, 22, 23
Rum Jungle, NT, Australia	Paleoproterozoic	Cmsd + Mag + If	Qz + Tur ± Py	None	24
Aldan Shield, eastern Siberia, Russia	Paleoproterozoic	Cmsd + Gran	Qz + Tur	Fe + borate	25
Bergslagen district, central Sweden	Paleoproterozoic	Cmsd ± Mrhy ± Mcht	Qz + Tur ± Ms ± Py ± Gn ± Sp	Pb + Zn + Ag ± Cu ± Fe	26, 27
Kurkkionvaara, Sweden	Paleoproterozoic	Cmsd	Qz + Tur	Cu + Zn + Pb	28, 29
Papaskwasati Formation, QC, Canada	Paleoproterozoic	Cmsd	Qz + Tur ± Ilt	None	30
Animikie basin, MN, USA	Paleoproterozoic	Cmsd + Amph + If	Qz + Tur + Ab + Pl + Mag	Fe	31, 32
Rudkins Cu–Zn mine, Bagdad district, AZ, USA	Paleoproterozoic	Mvols ± Cmsd	Qz + Tur	Cu + Zn	33
Minas Gerais, southern Brazil	Paleoproterozoic	Cmsd	Qz + Tur + Pl + Ms + Chl	Fe; Au ± Pd ± Pt	34
Sibao Group, northern Guangxi, China	Paleoproterozoic	Cmsd ± Albt ± Cot	Qz + Tur	None	35
Liaohé Group, Liaoning and Jilin provinces, China	Paleoproterozoic	Cmsd ± Qfr ± Marb	Qz + Tur ± Bt ± Kfs ± Ab ± Amp	Borate	36–39
Zhongtiaoshan, Shanxi province, China	Paleoproterozoic	Cmsd + Marb ± Albt	Qz + Tur	Cu	40
Rampura–Agucha Zn–Pb–Ag deposit, northern India	Paleoproterozoic	Cmsd ± Amph	Qz + Tur	Zn + Pb + Ag	41
Aravalli Supergroup, northwest India	Paleoproterozoic	Marb + Qtz ± Qfr	Qz + Tur ± Pl ± Ep ± Chl ± Pyh	Au ± Cu	42
Sargipalli Pb–Cu–Ag deposit, eastern India	Paleoproterozoic	Cmsd ± Marb	Qz + Tur ± Ms ± Gt ± Gr ± Gn	Cu + Pb + Ag ± Zn	43
Nagpur Cu–Zn district, central India	Paleoproterozoic(?)	Cmsd ± Amph	Qz + Tur	Cu ± Zn	44
Sullivan Pb–Zn–Ag mine, BC, Canada	Mesoproterozoic	Cmsd + Mgab	Qz + Tur	Pb + Zn + Ag	45, 46
Belt–Purcell supergroup, MT–ID–BC, USA–Canada	Mesoproterozoic	Cmsd ± Mgab	Qz + Tur	None; Pb + Zn + Ag	47, 48
Idaho cobalt belt, ID, USA	Mesoproterozoic	Cmsd ± If	Qz + Tur	Co + Cu ± Au	49, 50
Montaubon Zn–Pb–Cu–Ag–Au mine, QC, Canada	Mesoproterozoic	Cmsd + Amph	Qz + Tur + Gt + Ghn	Zn + Pb + Ag + Cu ± Au	51
Saint-Jovite, QC, Canada	Mesoproterozoic	Cmsd + Marb + Cot	Qz + Tur	Cu + Co ± Au	52
Bouchette, QC, Canada	Mesoproterozoic	Cmsd + Marb	Qz + Tur	Zn	53
Grenville Complex, NY, USA	Mesoproterozoic	Cmsd + Marb + Tles	Qz + Tur ± Py ± Sep ± Ab ± Mcc	None	54
Espleland Pb–Zn–Ag mine, southern Norway	Mesoproterozoic	Cmsd ± Amph	Qz + Tur	Pb + Zn + Ag	55
Serra do Itaberaba Group, southern Brazil	Mesoproterozoic	Mvols + Mcht ± If ± Mnr	Qz + Tur	None	56
Liuwu Cu–Zn mine, Sichuan province, China	Mesoproterozoic	Cmsd ± Amph	Qz + Tur	Cu + Zn + Co + Ag	57
Bushmanland Group, South Africa	Mesoproterozoic	Cmsd ± Fgn ± Amph	Qz + Tur + Sil + Ms ± Bt ± Crn ± Mag	Pb + Zn + Ag	58
Prieska Zn–Cu mine, Cape province, South Africa	Mesoproterozoic	Cmsd ± Amph	Qz + Tur ± Phl ± Ab ± Ged	Zn + Cu ± Ag	59, 60
Larseman Hills, East Antarctica	Mesoproterozoic	Cmsd	Qz + Tur + Ap	None	61
Peloritani Mountains, Sicily, Italy	Neoproterozoic	Cmsd ± Marb ± Amph	Qz + Tur ± Ab ± Ms ± Chl	Pb + Zn + Ag ± Cu; W	62
Damara orogen, northern Namibia	Neoproterozoic	Cmsd ± Csil	Qz + Tur ± Py ± Ccp ± Sch	None; W	63, 64
Damara orogen, central Namibia	Neoproterozoic	Sst + Dol + Absc	Qz + Tur + Ab	None	65, 66
Gartiep belt, southern Namibia	Neoproterozoic	Dol + Cpel + Albt ± Mcht	Qz + Tur ± Ab ± Dol ± Mrbk ± Tlc	None	67
Brusque Group, southern Brazil	Neoproterozoic	Cmsd ± Amph ± Scil	Qz + Tur ± Amp ± Py ± Mag	None	68

Sierras Pampeanas, central Argentina	Neoproterozoic–Cambrian	Cmsd ± Amph ± Cot	Qz + Tur ± Ms ± Py ± Pl	W	69, 70
Svratka Unit, eastern Czech Republic	Neoproterozoic–Cambrian	Cmsd + Marb ± Mrhy	Qz + Tur + Ms ± Bt ± Gt ± Ky	None	71, 72
Central Iberian zone, central Spain	Neoproterozoic–Cambrian	Cmsd ± Csil	Qz + Tur ± Pl ± Ms ± Bt	W	73, 74
Menderes Massif, southwest Turkey	Neoproterozoic–Cambrian	Cmsd ± Mrhy	Qz + Tur	None	75, 76
Austroalpine Complex, southern Austria	Early Paleozoic	Cmsd + Amph + Csil	Qz + Tur + Pl ± Gt ± Ms	W	77
Apuane Alps, northern Italy	Early Paleozoic	Cmsd + Mrhy	Qz + Tur ± Ms ± Cb ± Pyh ± Py	Pb + Zn + Ag ± Cu	78–80
Arzberg Series, southern Germany	Early Paleozoic	Cmsd + Marb	Qz + Tur	None	81
Großneiß Series, western Hungary	Early Paleozoic	Cmsd	Qz + Tur ± Ms ± Ky ± Chl	None; W	82
Pirén Alto Cu–Zn deposit, southern Chile	Early Paleozoic	Cmsd + Mvol ± Mcht	Qz + Tur	Cu ± Zn	83, 84
Black Hawk Zn–Cu mine area, ME, USA	Early Paleozoic	Cmsd + Gran	Qz + Tur ± Po ± Chl	Zn + Cu + Pb + Ag	85, 86
West Penobscot Bay area, ME, USA	Cambrian	Cmsd	Qz + Tur	None	85
Chopawamsic Formation, VA, USA	Ordovician	Mvole ± If	Qz + Tur	Cu + Zn	87
New Georgia Group, GA, USA	Ordovician	Mvole + Cmsd ± If	Qz + Tur	Cu + Zn	88
Central Piedmont province, SC, USA	Ordovician(?)	Cmsd + Cot ± If	Qz + Tur	Fe	89, 90
Ribband Group, southeast Ireland	Ordovician	Cmsd ± Amph	Qz + Tur ± Ms ± Bt	Pb + Zn; W; Au	91, 92
Cabeza de las Viñas Formation, western Spain	Ordovician	Cmsd + Amph	Qz + Tur	None	93
Tisová Cu–Co–Au mine, Czech Republic	Ordovician(?)	Cmsd ± Amph ± Gran	Qz + Tur	Cu ± Zn ± Pb	94
Vertiskos Formation, northern Greece	Silurian	Cmsd ± Amph	Qz + Tur	None	95
Elizabeth Cu mine, VT, USA	Devonian	Cmsd ± Amph	Qz + Tur ± Ab ± Pyh ± Gr	Cu ± Zn; none	86, 96
Ely Cu mine, VT, USA	Devonian	Cmsd ± Amph	Qz + Tur	Cu ± Zn	86, 96
Yindongzi–Tongmugou Pb–Zn mines, Qimling, China	Devonian	Cmsd ± Albt + Sct	Qz + Tur + Ab ± Brt ± Bt ± Sep	Pb + Zn + Ag ± Cu	97
Betic Cordillera, southeastern Spain	Devonian	Cmsd + Gran ± Marb	Qz + Tur ± Ms ± Bt ± Ep ± Gt	None	98
Ceinceo Villas massif, southern Spain	Permian–Triassic	Cmsd	Qz + Tur ± Pl ± Ms ± Chl ± Py ± Pyh	Pb + Zn	99
Bielwututu, Inner Mongolia, China	Carboniferous	Mvole ± Cmsd	Qz + Tur	Cu ± Zn	100, 101
Attic–Cycladic crystalline complex, Andros, Greece	Carboniferous	Cmsd + Cot	Tur + Qz + Ms + Hem	None	102
Otago Schist, western New Zealand	Triassic	Cmsd	Qz + Tur + Ms ± Pmt	None; W	103
<sup>1</sup> Key to province and state abbreviations: AZ, Arizona; BC, British Columbia; GA, Georgia; ID, Idaho; ME, Maine; MN, Minnesota; MT, Montana; NSW, New South Wales; NT, Northern Territory; NY, New York; QC, Québec; SA, South Australia; SC, South Carolina; VA, Virginia; VT, Vermont; WA, Western Australia.					
<sup>2</sup> Host rock abbreviations: Absc, albite–scapolite rock; Alb, albite; Amph, amphibolite; Brt, barite; Cmsd, clastic metasediments; Cot, cotecule (spessartine–quartz rock); Cpel, calcareous pelite; Csil, calc–silicate; Dol, dolostone; Fgn, felsic gneiss; Gran, granite; If, iron formation; Mag, magnetite; Marb, marble; Mbas, metabasalt; Mcarb, metacarbonate; Mcht, metachert; Mevp, metacavortite; Mgab; metagabbro; Mrhy, metarhyolite; Mnr, Mn–rich rock; Mumv, meta–ultramafic volcanic; Mvole, metavolcanic felsic + mafic; Qfr, quartz–feldspar rock; Qtzt, quartzite; Sct, scapolite–biotite rock; Sst, sandstone; Tles, tale schist.					
<sup>3</sup> Mineral abbreviations (Warr 2021): Ab, albite; Amp, amphibole; Ap, apatite; Ath, anthophyllite; Brt, barite; Bt, biotite; Cb, carbonate; Cep, chalcopyrite; Chl, chlorite; Cm, corundum; Dol, dolomite; Ep, epidote; Ged, gedrite; Gln, garnet; Gt, garnet; Hbl, hornblende; Hem, hematite; Il, illite; Kfs, K–feldspar; Ky, kyanite; Mcc, microcline; Mrbk, magnesio–riebeckite; Ms, muscovite; Mag, magnetite; Pl, plagioclase; Pnt, piemontite; Py, pyrite; Qz, quartz; Sch, scheelite; Sep, scapolite; Sil, sillimanite; Sp, sphalerite; Sps, spessartine; Tle, tale; Tur, tourmaline.					
<sup>4</sup> References: 1, Appel (1995); 2, Beyerly and Palmer (1991); 3, Farber et al. (2015); 4, Ota et al. (2019); 5, Appel (1988a); 6, Appel (1988b); 7, Appel (1988c); 8, Appel (1992); 9, Appel and Garde (1987); 10, Riehl and Cabral (2018); 11, Cunningham et al. (1973); 12, Ndiaye and Guillou (1997); 13, Slack et al. (1993); 14, Barnes (1983); 15, Barnes (1988); 16, Slack et al. (1984); 17, Ito and Plimer (1987); 18, Plimer (1988); 19, Spry and Teale (2021); 20, McGloin et al. (2016); 21, McGloin (2017); 22, Nicholson (1980); 23, Plimer (1986); 24, Bone (1988); 25, Mitich (1946); 26, Hellingwerf et al. (1988); 27, Hellingwerf et al. (1994); 28, Niimiskorpi (1986); 29, Frietsch (1991); 30, Chown (1987); 31, Boerboom (1989); 32, Cleland et al. (1996); 33, Conway (1986); 34, Cabral et al. (2011); 35, Mao (1995); 36, Peng and Palmer (1995); 37, Jiang et al. (1997); 38, Peng and Palmer (1995); 39, Xu et al. (2004); 40, Sun and Ge (1989); 41, Höller and Gandhi (1997); 42, Golani et al. (2002); 43, Vishwakarma (1996); 44, Bandyopadhyay et al. (1993); 45, Ethier and Campbell (1977); 46, Slack et al. (2000b); 47, Slack (1993); 48, Jiang et al. (2000a); 49, Modreski and Connor (1991); 50, Bookstrom et al. (2016); 51, Bernier et al. (1987); 52, Nantel (1994a); 53, Nantel (1994b); 54, Brown and Ayuso (1985); 55, Petersen et al. (1995); 56, Juliani et al. (2000); 57, Mao et al. (1995); 58, Willner (1992); 59, Wagener and van Schalkwyk (1986); 60, Theart et al. (1989); 61, Grew et al. (2013); 62, Ferla and Meli (2007); 63, Badenhorst (1988); 64, Steven and Moore (1995); 65, Behr et al. (1983); 66, Henry et al. (2008); 67, Frimmel and Jiang (2001); 68, Garda et al. (2013); 69, de Brodtkorb et al. (1985); 70, Tourn et al. (2004); 71, Houzar et al. (1998); 72, Čopíjaková et al. (2009); 73, Pesquera et al. (2005); 74, Pesquera et al. (2009); 75, Mittwede et al. (1992); 76, Bozkurt et al. (2006); 77, Raith (1988); 78, Benvenuti et al. (1989); 79, Benvenuti et al. (1991); 80, D’Orazio et al. (2017); 81, Abraham et al. (1972); 82, Spráncz et al. (2018); 83, Schira et al. (1990); 84, Collao et al. (1990); 85, Slack (1980); 86, Taylor and Slack (1984); 87, Pavlides et al. (1982); 88, Abrams and McConnell (1984); 89, Mittwede (1984); 90, Mittwede (1990); 91, McArdle et al. (1989); 92, McArdle and Kennan (1992); 93, Fernández and Moro (1992); 94, Pertold et al. (1994); 95, Michailidis and Kassoli–Fourmaraki (1994); 96, Slack et al. (2001); 97, Jiang et al. (1995); 98, Torres–Ruiz et al. (2003); 99, Pesquera and Velasco (1997); 100, Nie et al. (1990); 101, Nie (1993); 102, Reinecke et al. (1985); 103, Hutton (1939).					

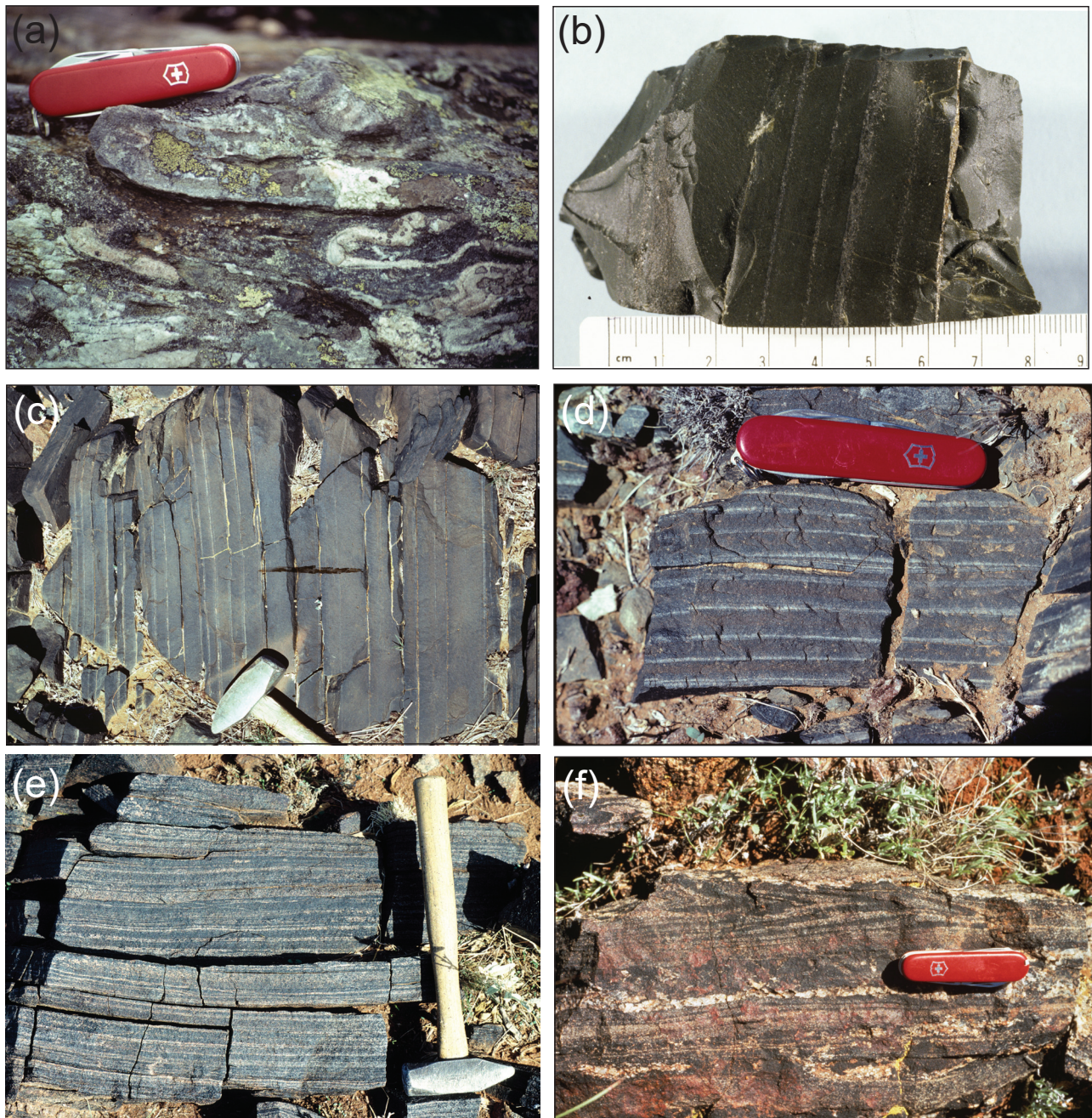


**Fig. 2** Field photographs of selected tourmalinites. **a** – Folded coticule (resistant beds) and interlayered tourmalinite (black), southeast Ireland. **b** – Hand specimen of cherty tourmalinite from the shallow footwall of Sullivan Pb–Zn–Ag deposit, Canada. **c** – Fine-grained massive tourmalinite from northern Broken Hill block, Australia. **d** – Graded beds in fine-grained tourmalinite from northern Broken Hill block. **e** – Layered coarse-grained tourmalinite from northern Broken Hill block. **f** – Isoclinal fold in tourmalinite (above the knife) from central Broken Hill block.

Paleozoic sequences of the Appalachian–Caledonian orogen (Kennan and Kennedy 1983; Slack et al. 1984).

### 2.3. Structures, textures, and mineral assemblages

Field aspects of tourmalinites vary widely partly as a function of superimposed metamorphic grade. For example, cherty tourmalinites characterize lower greenschist-

facies strata of the Belt–Purcell Supergroup including in the footwall of the Sullivan Pb–Zn–Ag deposit (Fig. 2b). Other tourmalinites, however, are massive without obvious sedimentary structures (Fig. 2c). Rarely observed are small tourmaline-quartz veinlets that are clear feeders to stratigraphically overlying tourmalinites (Fig. 3a). Prominent sedimentary structures include graded beds, cross-laminations, flames, and rip-up clasts (Ethier and Campbell 1977; Slack et al. 1984, 2000b; Badenhorst

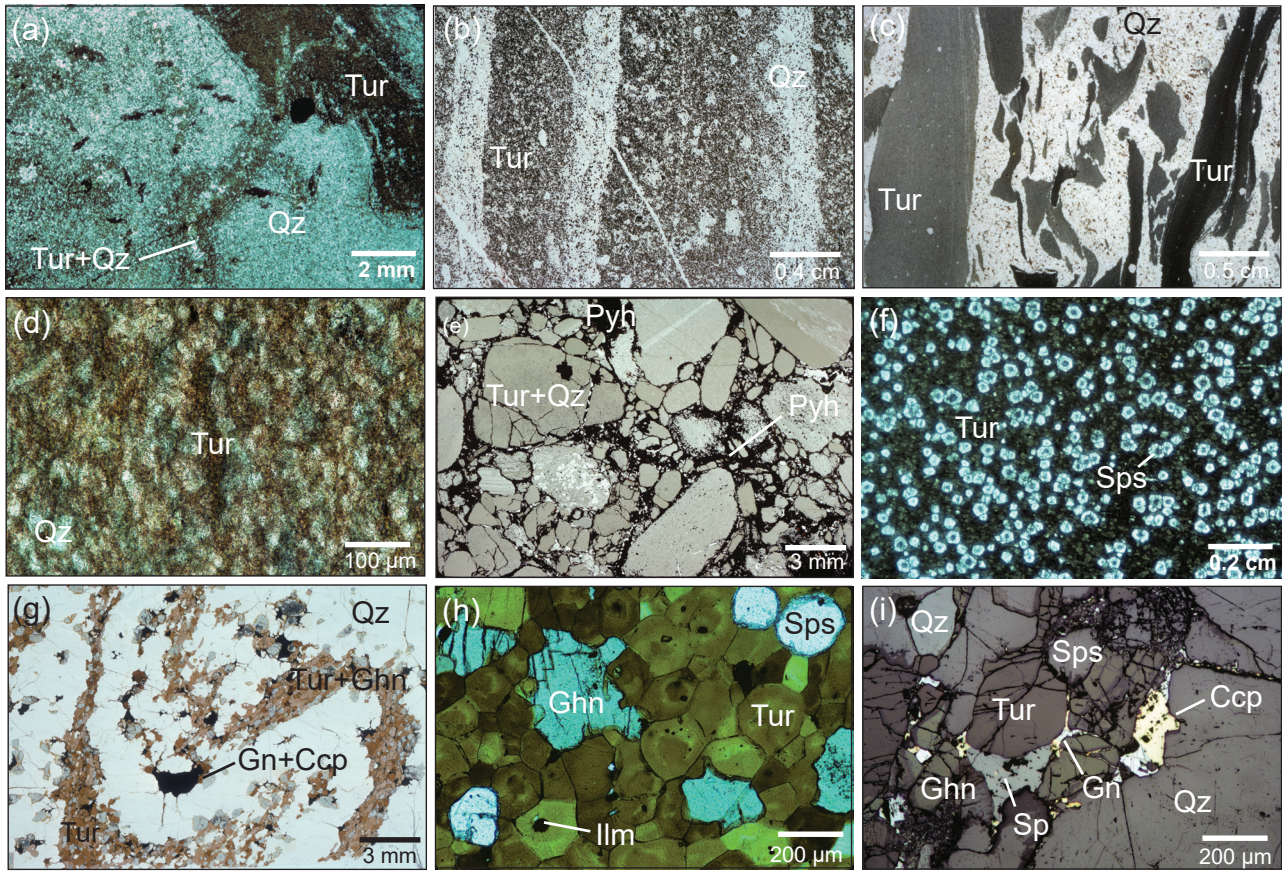


**Fig. 3** Photomicrographs of tourmalinites (all plane-polarized transmitted light unless noted otherwise). **a** – Irregular quartz-tourmaline vein in partly tourmalinized siltstone feeding overlying tourmalinite, Fork locality, northwestern Montana. **b** – Graded bedding in stratiform tourmalinite, Black Prince Pb–Zn–Ag deposit, Broken Hill district, showing fine-grained tourmaline concentrations in tops of beds (stratigraphic tops to left). **c** – Tourmaline-rich rip-up clasts in stratiform tourmalinite, Mt. Mahon locality, southeastern British Columbia; note lack of tourmaline in the quartz-rich matrix. **d** – Fine-grained tourmalinite from the deep footwall of Sullivan Pb–Zn–Ag deposit, showing abundant small (< 20 µm long) needles of tourmaline and partially replaced grains of detrital quartz. **e** – Tourmalinized sedimentary fragmental rock (mud volcano deposit) from the shallow footwall of Sullivan Pb–Zn–Ag deposit, showing microcrystalline tourmaline (grey) in quartz-rich clasts and abundant matrix pyrrhotite. **f** – Garnet-rich tourmalinite from tourmalinite from the shallow footwall of Sullivan Pb–Zn–Ag deposit, showing tourmaline cores in spessartine-rich garnets; whole-rock MnO = 3.5 wt. %. **g** – Folded quartz-tourmaline-sulfide tourmalinite from Globe Pb–Zn–Ag mine, Broken Hill district. **h** – Typical stratiform tourmalinite from Globe Pb–Zn–Ag mine, Broken Hill district, showing zoned tourmaline with minor spessartine, gahnite, and sulfides (black). **i** – Sulfides in Globe mine tourmalinite (reflected light). Abbreviations: Ccp, chalcopyrite; Gn, galena; Ghn, gahnite; Ilm, ilmenite; Pyh, pyrrhotite; Qz, quartz; Sp, sphalerite; Sps, spessartine; Tur, tourmaline.

1988; Stevens and Bradley 2018). These structures may be present even in tourmalinites that have been metamorphosed to upper amphibolite grade, on macroscopic and microscopic scales (Fig. 2d, 3b, 3c). However, graded beds, cross-laminations, and rip-up clasts do not require an early (syngenetic) formation of tourmaline, because similar structures are easily formed by the selected replacement of aluminous beds or laminae during diagenesis and metamorphism. This process may include the formation of rip-up clasts of tourmalinite in a tourmaline-free matrix, by which boron-bearing fluids preferentially replace aluminous clasts but not the typically quartzose and Al-free matrix (Fig. 3c). Moreover, in areas where the stratigraphic younging direction is known, the typical concentration of tourmaline in the tops of graded beds (Fig. 3b) is inconsistent with a purely syngenetic process,

such as deposition from hydrothermal plumes or density currents, because tourmaline has a much higher specific gravity than quartz (~3.1 and 2.65, respectively) and would settle first. In deformed and metamorphosed terranes, tourmalinites may also display layered structures (Fig. 2e) and various styles of folding, including isoclinal folds (Fig. 2f).

Textures of tourmaline in tourmalinites vary widely. In weakly metamorphosed terranes, tourmaline grains typically are ~50 to 200 µm in diameter. However, in some areas, the grains are very small (~5–50 µm), as in the Belt-Purcell Supergroup (Fig. 2b, 3d; Ethier and Campbell 1977; Slack 1993), the Barberton greenstone belt (Byerly and Palmer 1991), and the Yindongzi-Tongmugou Pb–Zn deposits in China (Jiang et al. 1995). Tourmaline in such terranes is characteristically ran-

domly oriented, consistent with static growth, and may be euhedral or anhedral, and optically zoned or unzoned. In contrast, tourmalinites within moderately deformed and metamorphosed sequences commonly have optically zoned and aligned tourmaline prisms as much as 1 to 3 cm in length, as in the Bohemian massif (Čopjaková et al. 2009). In some cases, optical and chemical zoning patterns observed in these settings indicate partial dissolution of primary tourmaline and overgrowth of new tourmaline with a composition stable under the attendant metamorphic conditions. Tourmalinite-hosted tourmaline grains in very high-grade terranes at upper amphibolite or granulite facies are distinctive in being granoblastic and unzoned or optically zoned, as in the Grenville Complex of New York State (Brown and Ayuso 1985) and in the southern part of the Broken Hill block of Australia (Slack et al. 1993), consistent with recovery and coarsening at high-grade followed by little to no retrograde effects. Fine-scale oscillatory and sector zoning in tourmaline from tourmalinites is uncommon relative to that in massive sulfides and other hydrothermal ores, probably due to the much higher fluid flux involved in the formation of these ore deposits (cf. Taylor and Slack 1984; Slack 1996; Slack et al. 1997). For example, in the footwall tourmalinite pipe of the Sullivan Pb–Zn–Ag deposit, tourmaline locally forms concentric growth zones within small (2 mm) euhedral quartz crystals (Jiang et al. 1998, Fig. 3a), attesting to the hydrothermal origin of this tourmaline.

Mineral assemblages of tourmalinites are dominated by tourmaline and quartz (Tab. 1). Characteristic are alternating tourmaline- and quartz-rich layers or laminae. In most cases, tourmaline overall is modally subequal to quartz, but in others, the tourmaline may constitute up to 90 vol. % of the rock. Muscovite, plagioclase, and chlorite occur in many samples. Less common phases in tourmalinites are biotite, apatite, amphibole, carbonate, graphite (or carbonaceous material), garnet, K-feldspar, magnetite, scapolite, ilmenite, and rutile. Sulfide-bearing samples typically contain pyrite and/or pyrrhotite, in some cases sphalerite, galena, or chalcopyrite. The Zn-spinel gahnite is volumetrically important in metamorphosed tourmalinites associated with Zn–Pb–Ag deposits at Montauban in Québec (Bernier et al. 1987) and in several deposits in the Broken Hill district (Barnes 1988; Slack et al. 1993).

Tourmaline is mechanically and chemically very stable and thus is commonly retained even in high-grade metamorphic terranes (e.g., Marschall et al. 2009; van Hinsberg et al. 2011). For example, stratiform tourmalinites are well preserved in granulite-facies rocks of the Broken Hill district and the Larsemann Hills of East Antarctica (Slack et al. 1993; Grew et al. 2013). As Marschall et al. (2009) discussed, the upper stability limit of tourma-

line depends on several factors, including temperature, pressure, and fluid composition. The complete prograde breakdown has been described in the migmatite zone of the Ryoke metamorphic belt in Japan, involving the reaction of tourmaline to sillimanite + cordierite (Kawakami 2001). On the retrograde path, within the two-pyroxene granulite zone at Broken Hill, small (< 1 cm) domains in partially retrogressed tourmalinites locally show evidence of a breakdown reaction of tourmaline to muscovite + B-rich biotite + staurolite + corundum ± margarite (Slack and Robinson 1990). In some low-grade metamorphic terranes, such as in wall rocks of the Sullivan Pb–Zn–Ag deposit, tourmalinite-hosted tourmaline is replaced locally by chlorite, muscovite, or albite (Leitch and Turner 1992). The breakdown of tourmaline during metamorphism likely reflects the incursion of B-undersaturated fluids with a relatively high pH (Slack 1996).

### 3. Metallogeny

#### 3.1. Base-metal deposits

The major deposit types spatially associated with pre-metamorphic stratabound tourmalinites are VMS and CD Zn–Pb (Figs 1a, 1b). In both types of deposits, stratiform tourmalinites commonly form beds or lenses up to 1 m thick in the stratigraphic footwall and/or hanging wall of the orebodies, or lateral equivalents along strike. In VMS deposits, tourmalinites may be interbedded with iron formation, metachert, and cotecule, or occur in wall rocks and surrounding country rocks. At the Elizabeth Cu deposit in Vermont, USA (Slack et al. 2001) and the Prieska Cu–Zn deposit in South Africa (Theart et al. 1989), tourmalinites form stratigraphic units in contact with massive sulfide or in adjacent metavolcanic and metasedimentary rocks. Appreciable tourmaline, although insufficient to be tourmalinite, also occurs as crystals within massive sulfide at many deposits (Slack 1982, 1996).

Although not stratiform, stratabound alteration zones in some sediment-hosted deposits can have abundant tourmaline. A key example is in the footwall tourmalinite pipe of the large Sullivan CD Pb–Zn–Ag deposit in British Columbia (Fig. 4) that contains ca. 20 to 60 vol. % tourmaline and extends at least 600 m beneath the central part (vent complex) of the orebody (Slack et al. 2000b). This pipe is distinctive in also containing both black and brown tourmalinites as veins that cut each other, very fine-grained tourmaline (Figs 2b, 3d), and tourmalinized conglomerates (Fig. 3e). Similar tourmalinite pipes and overlying sulfide zones have been described from other deposits in the Belt–Purcell Supergroup, as at the Fors prospect (Höy et al. 2000). The shallow footwall beneath the Sullivan orebody also contains thin stratiform units

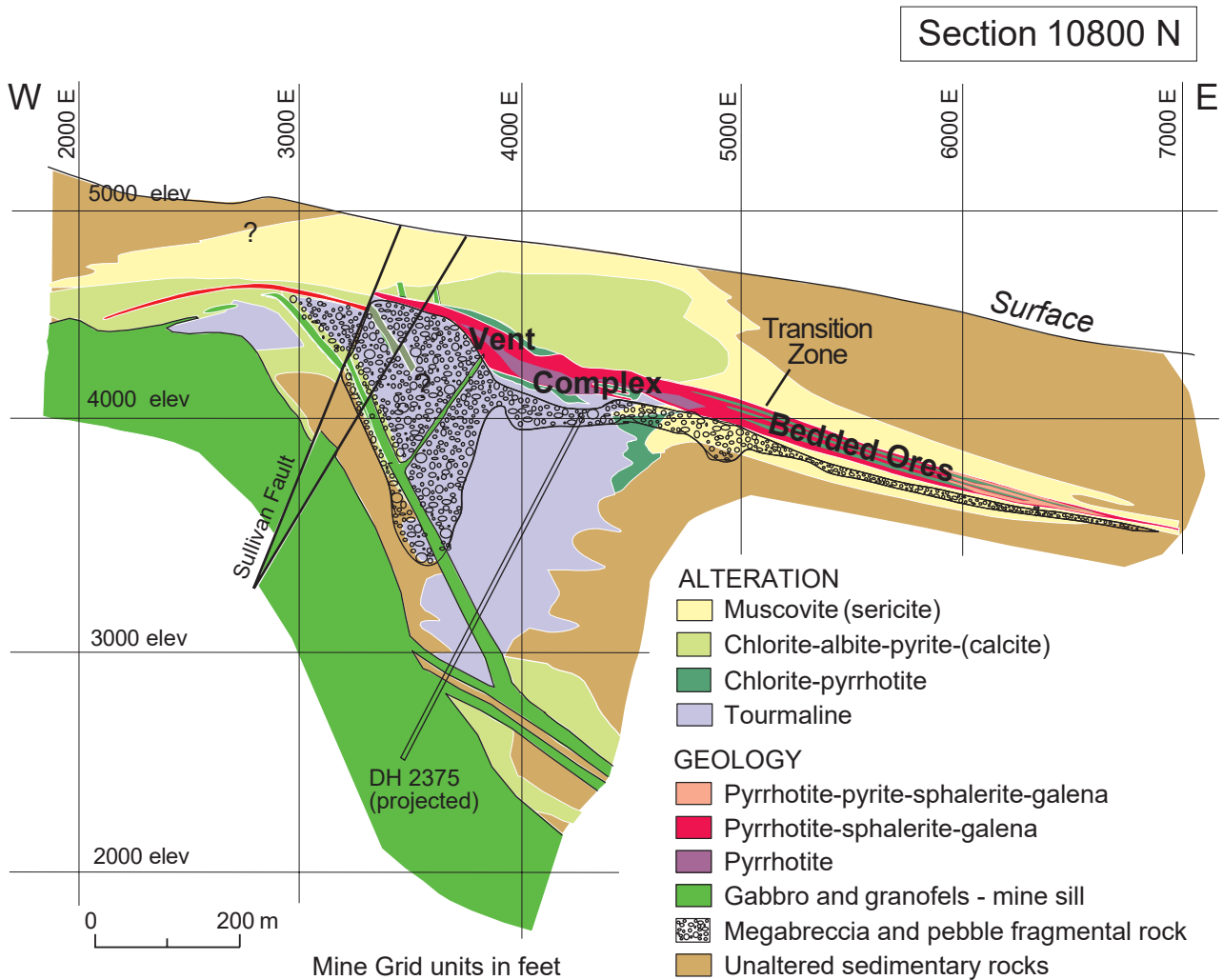


**Fig. 4** Geological cross-section of Sullivan Pb–Zn–Ag deposit showing the distribution of major footwall and minor hanging-wall tourmalinites below and above sulfide ore zones. Modified from Lydon (2007).

of interlayered tourmalinite and sulfides, laminae of sphalerite + galena ± pyrrhotite within tourmalinite (Slack et al. 2000b), and spessartine-rich tourmalinite (Fig. 3f). At the Globe Pb–Zn–Ag deposit in the Broken Hill district (Fig. 5), many tourmalinites occur stratigraphically close to the sulfide lodes, including quartz-rich variants with minor sulfides that display fold structures (Fig. 3g), variants with abundant gahnite and spessartine (Fig. 3h), and sulfide-rich variants that contain sphalerite + galena ± chalcopyrite (Fig. 3i). The small sediment-hosted Black Prince Pb–Zn–Ag deposit, in the northern part of the Broken Hill district, has a footwall tourmalinite pipe like that at the Sullivan deposit (Slack et al. 1993).

### 3.2. Borate deposits

Well-documented stratabound tourmalinites associated with borate deposits are restricted to northeast China Liaoning and Jilin provinces. A similar association in

Paleoproterozoic strata of the Aldan Shield in eastern Siberia was described by Mitich (1946), but limited data available for this occurrence preclude a meaningful interpretation. The deposits in China, occurring within Paleoproterozoic rocks intermittently over a distance of ca. 300 km, comprise Mg and Mg–Fe borate minerals within magnesian marble, Mg-silicate rock, and quartz-feldspar rock (Jiang et al. 1997; Peng and Palmer 1995, 2002; Xu et al. 2004). An unanswered question is how the Mg-rich borate minerals in these Paleoproterozoic deposits survived greenschist-facies metamorphism (Peng and Palmer 1995), given the very high solubility of such minerals in Tertiary and younger deposits (e.g., Crowley 1996; Helvacı and Ortı 2004). One possible explanation is that these borate deposits and related tourmalinites are not of evaporitic origin but instead formed by skarn-type metasomatic processes during the emplacement of nearby granites and granitic pegmatites (cf. Peng and Palmer 1995). Alternatively, these mineralogically complex de-

posits may have formed through the combined effects of multistage evaporation, metamorphism, and magmatism (Peng and Palmer 2002; Yan and Chen 2014; Hu et al. 2015).

### 3.3. Tungsten deposits

Some stratabound scheelite deposits are locally associated with tourmalinites (Barnes 1983; Arribas-Rosado 1986; Plimer 1987; Appel 1988a; Raith 1988; Leake et al. 1989). Although most workers have generally invoked syngenetic or diagenetic origins for the scheelite and tourmalinites, major uncertainty nevertheless surrounds the timing of both the tungsten and boron mineralization. For example, geological, textural, and mineral-chemical data for the scheelite-bearing tourmalinites of the eastern Alps of Hungary led Spránitz et al. (2018) to reject a premetamorphic model and instead invoke a granite-related metasomatic origin. This interpretation is consistent with the lack of associated chemical metasedimentary rocks like iron formation and coticule with these tourmalinites. Notably, all tungsten-associated tourmalinites described in the literature lack these and other chemical metasediments (Tab. 1). Also relevant in this context are the uniformly low contents of tungsten ( $<500 \mu\text{g/g}$ ) in ancient VMS and CD Zn–Pb deposits associated with tourmalinites (e.g., Slack et al. 1993, 2000a, b), and the even lower concentrations of this metal in

modern VMS deposits ( $\leq 100 \mu\text{g/g}$ ; Hannington 2014) as well as in metalliferous sediments of the Red Sea ( $\leq 10 \mu\text{g/g}$ ; Hendricks et al. 1969). On balance, therefore, it seems unlikely that high tungsten concentrations form by premetamorphic hydrothermal processes together with tourmalinites, either by syngenetic processes on or near the seafloor or during diagenesis in the subsurface. More field-based research is needed to fully evaluate the scheelite-tourmalinite connection and timing relative to local syngenetic, diagenetic, and metamorphic processes.

### 3.4. Gold deposits

Uncertain affinities and origins concern tourmalinites associated with stratabound gold deposits. In the past, the broadly stratabound nature of both led many workers to propose origins prior to deformation and metamorphism. A key example is the tourmalinite-hosted gold orebody at the Passagem de Mariana mine in Brazil that in early studies was attributed to syngenetic mineralization (Fleischer and Routhier 1973). However, recent work has convincingly shown this deposit to be an epigenetic, post-peak metamorphic vein that formed coevally with tourmalinization in a regional shear zone (Vial et al. 2007; Trumbull et al. 2019). A similar syn- to post-metamorphic origin was proposed by Kalbskopf and Barton (2003) for tourmalinite-hosted gold at the Zandrivier and other deposits in southern Africa. In contrast, tourmalinite

formation in some deposits may have predated gold mineralization, such as in the Loulo deposit in Mali, which was attributed to premetamorphic processes by Dommanget et al. (1993) but in light of more recent structural and geochemical data is likely related to late-orogenic magmatic processes (Lawrence et al. 2013). In northern Australia, stratabound gold deposits are associated with, and in places contained in, laterally extensive stratiform tourmalinites, such as

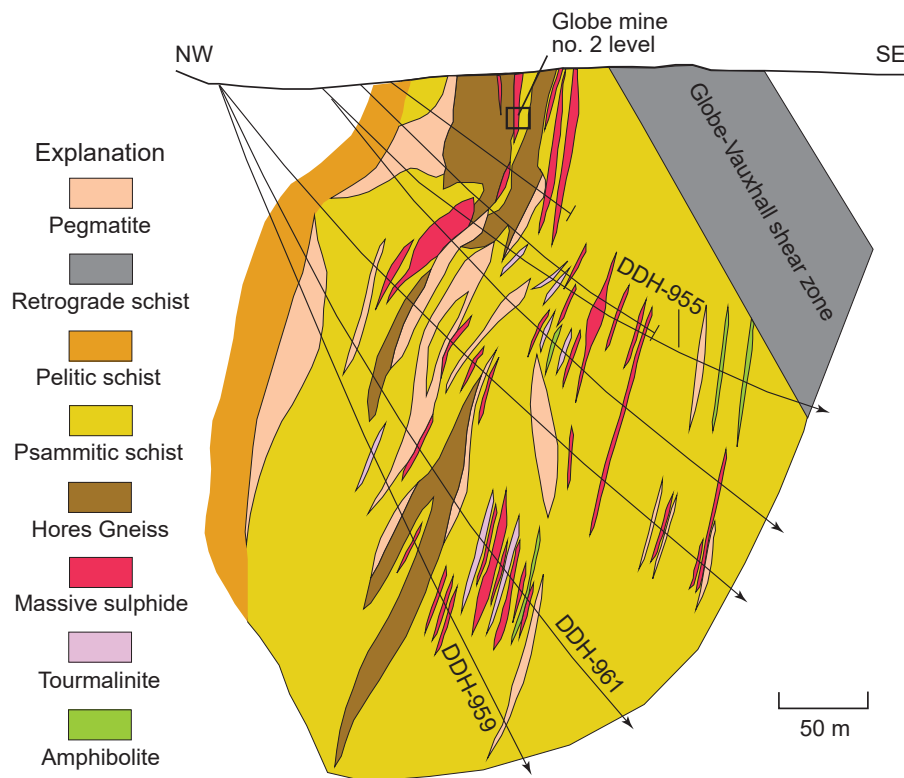


**Fig. 5** Geological cross-section of Globe Pb–Zn–Ag mine area at the northeast end of main Broken Hill Pb–Zn–Ag deposit. Note the proximity of most tourmalinites to sulfide zones. Hores (Potosi) Gneiss is interpreted to be a metamorphosed rhyolite tuff (Stevens and Bradley 2018). Selected drill holes are shown; tourmalinites from labeled holes were used for petrographic, microprobe, geochemical, and boron isotope analyses (Slack et al. 1993).

at the Good Shephard deposit in the Golden Dyke Dome (Nicholson 1980) and other gold deposits in the Pine Creek inlier (Plimer 1986). Importantly, the Golden Dyke tourmalinites, which have high whole-rock iron contents, are folded and cut by slaty cleavage (Slack 1996), consistent with a predeformational origin during diagenesis. This type of stratiform and extensive tourmalinite may be considered a receptive host rock that localized later gold mineralization, as proposed by Lambeck et al. (2011) for gold deposits in other iron-rich sedimentary rocks of the region. Tourmalinites may also be favorable hosts for gold mineralization by having a high mechanical competency that is conducive to localizing fractures and permeability for subsequent gold deposition (Lawrence et al. 2013). It remains to be seen whether some gold-bearing tourmalinites formed on or near the paleo-seafloor, which is a worthwhile topic for future studies.

#### 4. Geochemical signatures

##### 4.1. Whole-rock geochemistry

Many studies have reported on bulk composition of tourmalinites, including data for major, trace, and rare earth elements (REE). Contents of major elements in most cases reflect the composition and proportion of tourmaline, whereas trace element and REE concentrations

mainly record proportions of accessory detrital minerals such as monazite, ilmenite, rutile, and zircon. In hydrothermal systems that formed under relatively low fluid/rock ratios (i.e., rock-buffered), as recorded in tourmalinites from the Broken Hill district in Australia that formed distal to hydrothermal sources (Slack et al. 1993), major elements can be enriched or depleted relative to unaltered host metasediments; trace elements and most REE contents tend to be broadly similar, the latter having shale-normalized abundances similar to those of the unaltered host metasedimentary rocks (Fig. 6a). Net mass changes calculated for these tourmalinites, based on dual Al-normalization for each sample and for average unaltered metasedimentary host rock, show moderate losses only

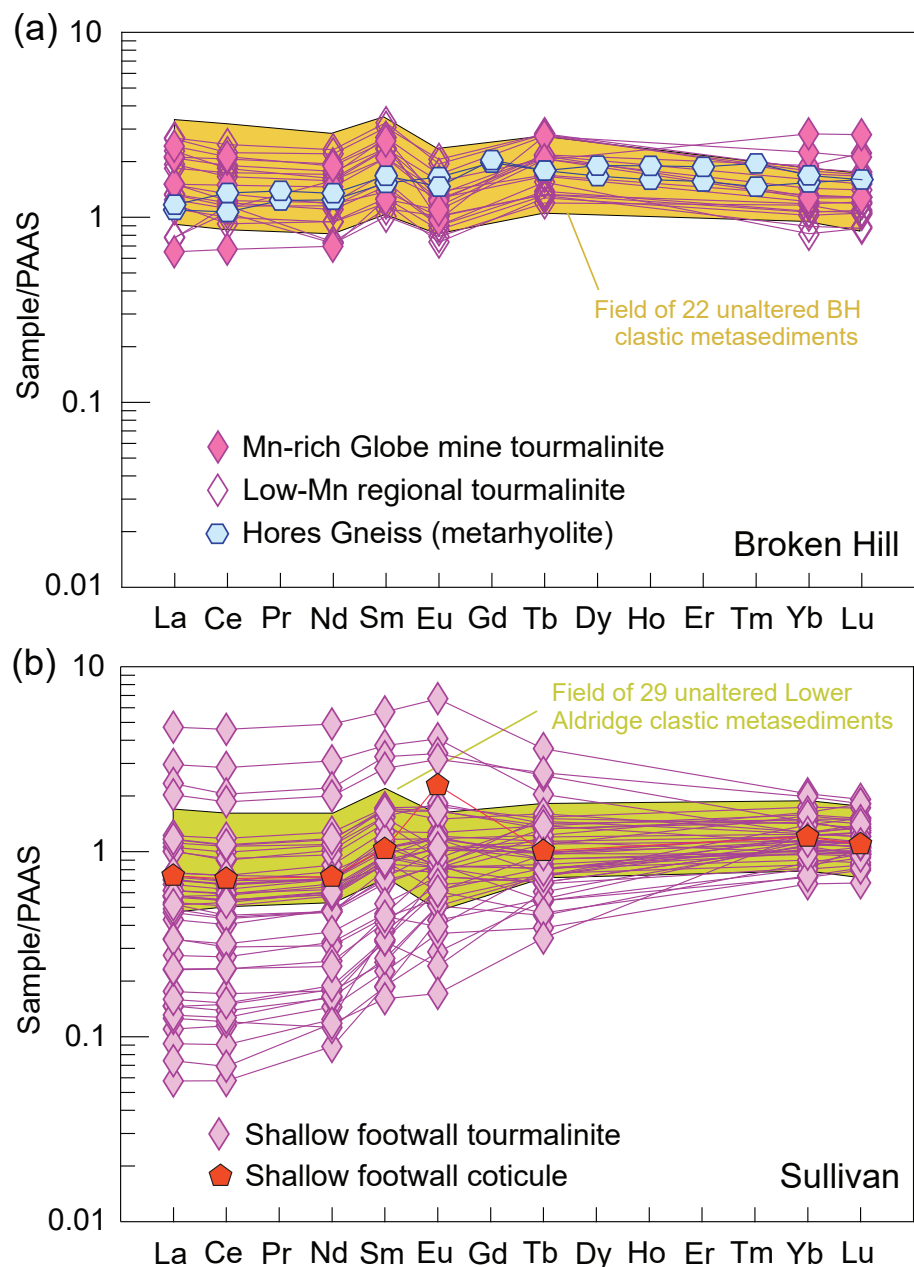


**Fig. 6** Shale-normalized REE data for tourmalinites and unaltered host metasedimentary rocks. (a) Distal tourmalinites and host rocks from Broken Hill district (Slack et al. 1993; Slack and Stevens 1994), the latter including local metarhyolite of the Hores Gneiss (Raveggi et al. 2008). (b) Proximal tourmalinites and host rocks from Sullivan Pb–Zn–Ag deposit (Slack et al. 2000b; Slack and Höy 2000). Distal tourmalinites are attributed to formation in low fluid/rock settings, whereas proximal tourmalinites formed in high fluid/rock settings (see text). Note that missing values for Pr, Gd, Dy, Ho, Er, and Tm for Sullivan and Broken Hill reflect acquisition by Instrumental Neutron Activation Analysis (INAA), which does not provide values for these REE; hence, calculations of Ce anomalies and Y/Ho ratios are not possible.

for Mn and Ca, and minimal differences for REE (Figs 6a, 7a). In other cases, however, variable mobility of major and trace elements, as well as light REE (LREE), have been reported (Pesquera and Velasco 1997; Raith et al. 2004; Čopjaková et al. 2013; Grew et al. 2013)

Tourmalinites that formed in high fluid/rock systems commonly differ in having highly variable bulk compositions. A key example comes from the footwall pipe of the Sullivan Pb–Zn–Ag deposit, for which bulk compositions of tourmalinites may be greatly enriched or depleted in certain major elements, trace elements, and LREE or middle REE (MREE) (Fig. 6b, 7b) relative to unaltered sedimentary host rocks of the area (Slack et al. 2000b). Data for the stratabound but non-stratiform deep footwall tourmalinites, collected from a long drill core 10 to 560 m below the sulfide ore zones, indicate average Fe and Mg gains of ~30 and 20 %, respectively, whereas Mn shows an average loss of 30 %. Large average losses of ~50 to 90 % are evident for Ca, Na, K, Li, Rb, Cs, Ba, LREE

and MREE. Minimal average losses of less than 10 % are shown by Si, high field strength elements (HFSE; Ti, Sc, Y, Zr, Hf, Nb, Ta, Th), and heavy REE (HREE). In contrast, shallow and mainly stratiform tourmalinites less than 10 m below the ore zones (Fig. 7b) record large average gains for Mn (180 %) and Mg (60 %), and a moderate average gain for Fe (20 %), accompanied by moderate to large average losses for Ca (50 %), Na (70 %), and K (90 %); Si, HFSE, and all REE (on average) show only small losses or gains of less than 10 %. Bulk Fe/(Fe+Mg) ratios of the deep vs. shallow footwall tourmalinites also vary locally, the highest ratios (0.45–0.58) occurring in a thick quartzite unit 175 to 305 m below the ore zones. The diversity of chemical losses and gains exhibited by the footwall tourmalinites at the Sullivan Pb–Zn–Ag deposit are compatible with a model involving focused hydrothermal flow under high fluid/rock conditions, by which the deep footwall samples record preferential leaching of alkali and alkaline earth elements, LREE, and

MREE, coupled with moderate Fe- and Mg-metasomatism, by the metasomatism of argillaceous sediments. In contrast, data for the shallow footwall tourmalinites, especially the major gains shown by Mn and Mg, suggest similar high fluid/rock conditions but with a significant input of evolved seawater (Mg) during subsurface metasoma-

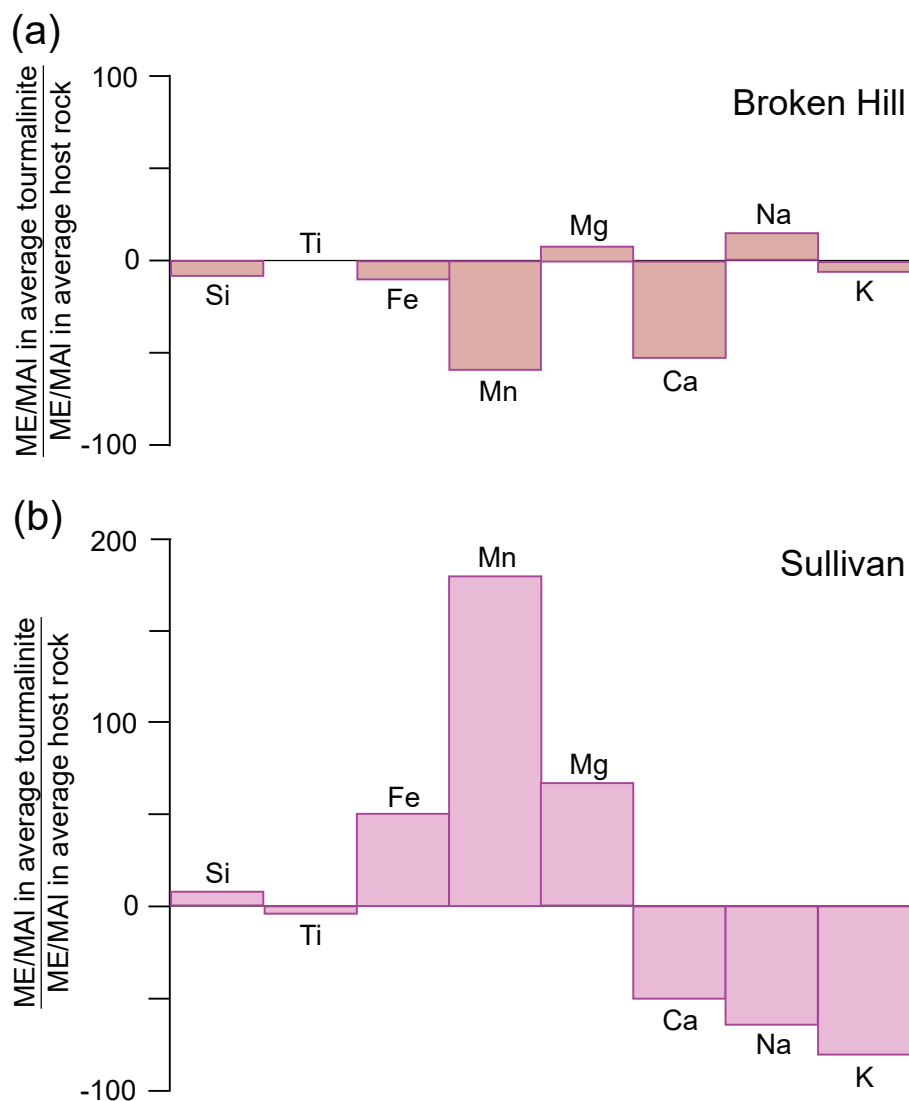


**Fig. 7** Metasomatic changes (shown in %) calculated for major elements during tourmalinite formation based on Al-normalization relative to that of unaltered host metasedimentary rocks. **a** – Distal low-Mn tourmalinites from Broken Hill district ( $n = 29$ ; Slack et al. 1993) compared to unaltered host rocks ( $n = 22$ ; Slack and Stevens 1994). **b** – Proximal tourmalinites from the shallow footwall of Sullivan Pb–Zn–Ag deposit ( $n = 41$ ; Slack et al. 2000b) compared to unaltered host rocks ( $n = 29$ ; Slack and Höy 2000). Tourmalinite data in A exclude those for Mn-rich tourmalinites in a deep part of this complex (see Fig. 4). Distal Broken Hill tourmalinites formed under low fluid/rock conditions, whereas proximal Sullivan tourmalinites in the shallow footwall formed via high fluid/rock ratios (see text). Abbreviations: ME, molar element; MAI, molar aluminum.

tism, together with exhalative venting and the deposition of Mn derived from a local hydrothermal plume. The inferred subseafloor processes in this shallow setting include major leaching of alkali and alkaline earth elements but no significant net changes in REE. However, the metasomatism there clearly remobilized LREE and MREE, at least on a local scale, as evidenced by the large range in PAAS-normalized abundances for these REE, relative to those for unaltered clastic metasedimentary host rocks of the area (Fig. 6a). Jiang (2000) also reported mobility of HFSE and U in the shallow footwall and hangingwall tourmalinites of the Sullivan deposit.

#### 4.2. Tourmaline compositions

Many studies have reported electron microprobe analyses (EMPA) for major and minor elements in tourmaline from tourmalinites. A comprehensive review of such data is beyond the scope of this paper, so the following is only a brief summary of published results. Overall, EMPA studies of such tourmalines from VMS and CD Zn–Pb deposits show compositions dominated by dravite–schorl with minor uvite and feruvite locally (Taylor and Slack 1984; Benvenuti et al. 1991; Slack et al. 1993; Jiang et al. 1995, 1998; Ferla and Meli 2007). Importantly, in some cases as at the Sullivan Pb–Zn–Ag deposit, compositions vary greatly depending on location relative to the ore zones (Jiang et al. 1998). Tourmalines in stratabound tourmalinites that lack associated metal concentrations are predominantly dravite–schorl in composition with minor proportions of the uvite or povondraite ( $\text{Fe}^{3+}$ -rich) endmembers (e.g., Pesquera and Velasco 1997; Tourn et al. 2004; Pesquera et al. 2005; Čopjaková et al. 2009; Yücel-Öztürk et al. 2015). Tourmaline compositions in such settings generally reflect the bulk host-rock chemistry of the precursor sediment (e.g., Slack 1996), but in high fluid/rock settings related to VMS and CD Zn–Pb deposits,  $\text{Fe}/(\text{Fe} + \text{Mg})$  ratios can vary greatly. For example, in unmetamorphosed to weakly metamorphosed deposits of this type, Mg-rich dravite can reflect a large seawater component in the hydrothermal fluids, whereas in highly metamorphosed deposits this tourmaline composition may also record sulfide-silicate reactions involving Fe-sulfides like pyrite and pyrrhotite (Slack 1996; Jiang et al. 1998; Slack and Trumbull 2011).

Metaevaporite-hosted tourmalinites contain a greater diversity of tourmaline compositions. In addition to dominant dravite or schorl components, and local uvite, many such tourmalines contain minor to major proportions of the oxy-dravite and povondraite endmembers, the latter distinguished by Na- and Mg-rich compositions that include significant  $\text{Fe}^{3+}$  substitution for  $\text{Al}^{3+}$  (Henry et al. 2008). Examples are Paleoproterozoic tourmalinites in northeast China (Jiang et al. 1997; Peng and Palmer

2002) and Neoproterozoic tourmalinites in the Gariep belt and Damara orogen of Namibia (Frimmel and Jiang 2001; Henry et al. 2008). As in the Namibian examples, the presence of a major povondraite component suggests that the tourmaline formed in an oxidizing environment from high-salinity fluids (Henry et al. 2008).

Data for trace elements and REE in tourmalinite-hosted tourmaline have been obtained by several methods. Early work by Taylor and Slack (1984) reported emission spectrographic data on untreated mineral separates, but in most samples, these results were variably affected by sulfide and other mineral inclusions. Jiang et al. (1997, 2000c) presented trace element and REE analyses of acid-leached tourmaline samples that also, in most cases, reflect the chemical influence of inclusions and intergrowths. The first *in situ* study on tourmalinites, by Griffin et al. (1996), used Proton-Induced X-ray Emission (PIXE) methods that revealed locally high contents of Zn (up to 2993  $\mu\text{g/g}$ ), Pb (up to 2379  $\mu\text{g/g}$ ), and Sr (up to 973  $\mu\text{g/g}$ ); elevated Zn and Pb values were measured on samples from or related to sulfide deposits including at Broken Hill. More recent *in situ* work has utilized laser ablation-inductively coupled plasma-mass spectrometry (LA-ICP-MS) that yields higher precision and accuracy for a much larger suite of elements than PIXE. Examples include Y + REE analyses of oxy-dravite and schorl cores of tourmalinite-hosted tourmaline grains from Neoproterozoic–Cambrian metasedimentary strata in the Bohemian Massif, the former type showing negative Eu but positive Y anomalies, and the latter both positive Eu and Y anomalies, attributed respectively to deposition predominantly from seawater and hydrothermal fluids (Čopjaková et al. 2013). Yan and Chen (2014) reported contrasting amounts of trace elements and REE in the cores and rims of tourmalines from tourmalinites in the Paleoproterozoic borate deposits of northeast China, and suggested that the cores formed by seafloor-hydrothermal processes with the rims reflecting syn-metamorphic growth. All of these TE and REE data are important in documenting the geochemical environments in which the tourmalines grew and in providing applications to mineral exploration, such as from grains with high concentrations of metals of economic interest (e.g., Slack 1982; Taylor and Slack 1984; Griffin et al. 1996). However, several caveats remain. One is the uncertainty in some cases (e.g., using LA-ICP-MS) whether high metal concentrations reflect submicroscopic inclusions, despite care in using time-resolved data reduction schemes. Another is the requirement when acquiring *in situ* data to know whether sector zones are being analyzed, because the *c*-sector can be enriched or depleted by a factor of up to 2 $\times$  in Li, Zn, Sr, and Sn relative to the *a*-sector that is compositionally unaffected by such zoning (van Hinsberg et al. 2017 and references therein). Also important is the

lack of published data on trace element fractionation between tourmaline and coexisting phases such as sulfides (e.g., Zn in sphalerite; Cu in chalcopyrite), oxides (e.g., Zn in gahnite), carbonates (e.g., Ca in calcite), and silicates (e.g., Zn in staurolite; REE in garnet and monazite). Only two studies have addressed this issue, one the empirical LA-ICP-MS work of Klemme et al. (2011) on the fractionation of trace elements and REE between tourmaline and muscovite in samples from the Broken Hill district. In a more detailed analysis of mineral chemistry in a granitic pluton in Spain, Pesquera et al. (2018) reported that, among coexisting silicates (1) tourmaline preferentially concentrates Be, Sr, and LREE; (2) Li, Rb,

Cs, Ba, Tl, W, HFSE, and HREE are incorporated into micas; and (3) metals such as Mn, Zn, Ni, Co, and Cu are preferentially incorporated into tourmaline instead of muscovite. In addition to these field-based studies, experimental work is needed on tourmaline-fluid fractionation under hydrothermal and not magmatic conditions, for an improved understanding of the potential uses – and pitfalls – of tourmaline chemistry in mineral exploration.

## 5. Stable isotopes

### 5.1. Oxygen and hydrogen

Early insights into the stable isotope compositions of tourmaline in massive sulfide deposits and tourmalinites were pioneered by Taylor and Slack (1984). Oxygen and hydrogen

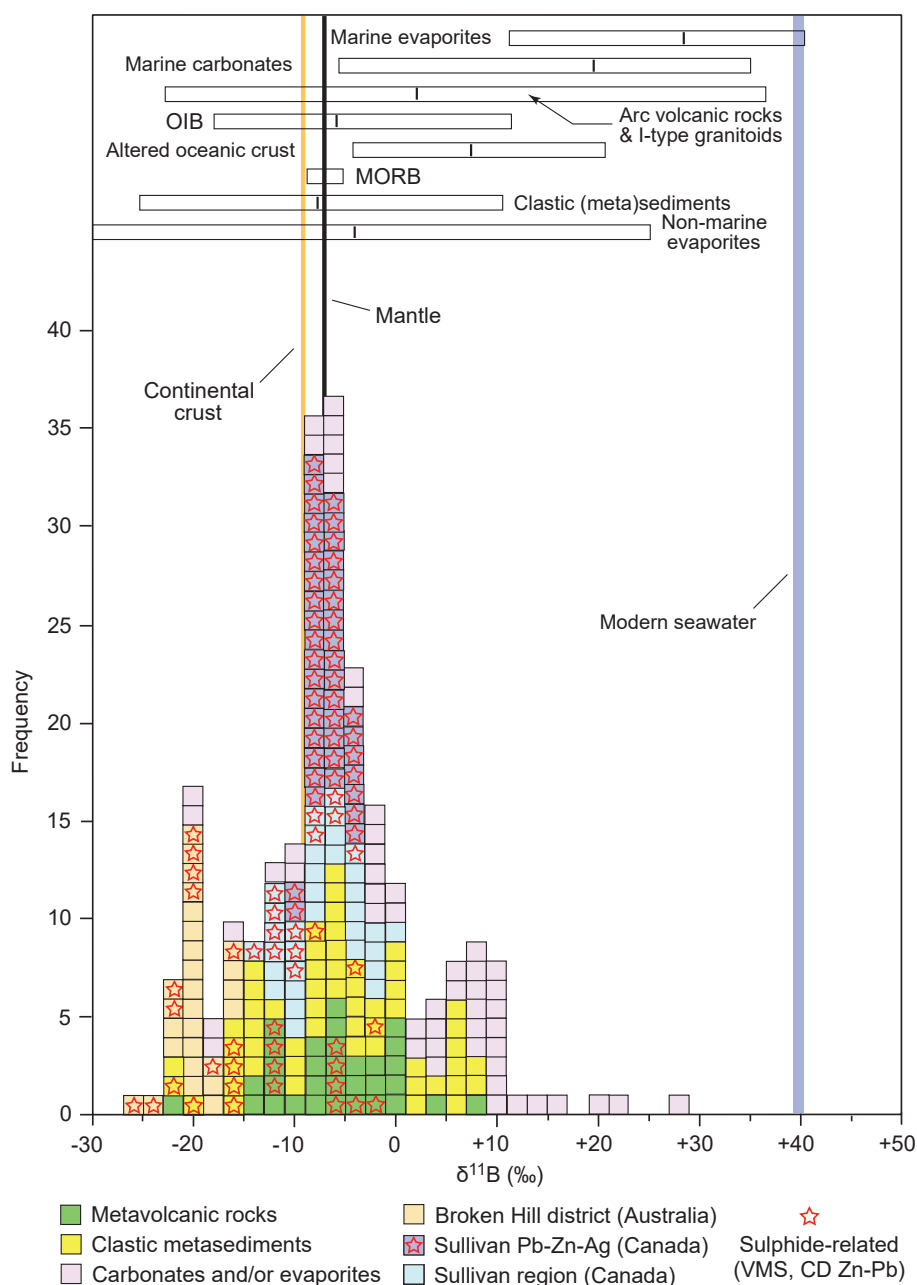


**Fig. 8** Histogram of boron isotope values ( $n = 243$ ) for tourmaline from stratabound tourmalinites of inferred premetamorphic origin with and without associated base-metal, iron, or borate mineralization. Not included are data for tourmaline from rocks containing <15 vol. % tourmaline, or for tourmalinites spatially associated with granites, pegmatites, quartz veins, faults and shear zones, or metamorphic replacements. Data for tourmalinites associated with gold mineralization are not shown. Multiple analyses of individual grains or portions of grains are averaged for each sample. Sources of data: Palmer and Slack (1989), Slack et al. (1989, 1993), Byerly and Palmer (1991), Bandyopadhyay et al. (1993), Peng and Palmer (1995, 2002), Jiang et al. (1995, 1997, 1999, 2000a), Chaussidon and Appel (1997), Jiang (2001), Frimmel and Jiang (2001), Xu et al. (2004), Tourn et al. (2004), Pesquera et al. (2005), Ferla and Meli (2007), Trumbull et al. (2008, 2011, 2019), Garda et al. (2010), Cabral et al. (2011), MacGregor et al. (2013), Yan and Chen (2014), Yücel-Öztürk et al. (2015), Farber et al. (2015), Grew et al. (2015), McGloin et al. (2019), Ota et al. (2019), Arena et al. (2020), Franz et al. (2021), Krmíček et al. (2021). Ranges of boron isotope values and median values (black vertical bars) for boron reservoirs from Marschall et al. (2017) and Trumbull et al. (2020). Abbreviations: CD, Clastic-Dominated; MORB, Mid-Ocean Ridge Basalt; OIB, Ocean-Island Basalt; VMS, Volcanogenic Massive Sulfide.

isotope data, obtained on tourmaline separates (only a few tourmalinites), yielded  $\delta^{18}\text{O}$  and  $\delta\text{D}$  values mainly in the range of +9.5 to +15.5 ‰ and -60 to -45 ‰, respectively. These values differ from those for pegmatite- and granite-hosted tourmalines, and suggest major influences on oxygen isotopes from host lithologies and on hydrogen isotopes from modified seawater. Note, however, that the D data for these samples are also consistent with a metamorphic fluid source that likely existed during metamorphically induced recrystallization of the tourmaline in these massive sulfide deposits (Slack 1996; Pesquera and Velasco 1997; Jiang 1998).

Analyses of oxygen and hydrogen isotopes in tourmalinite-hosted tourmalines from unmetamorphosed or weakly metamorphosed terranes can be especially informative such as in evaluating the role of evolved seawater in tourmaline formation. This approach has been used in several studies of tourmalinites from the Sullivan Pb–Zn–Ag deposit and enclosing Belt–Purcell Supergroup (Nesbitt et al. 1984; Beaty et al. 1988; Seal et al. 2000; Taylor et al. 2000). These studies reported  $\delta^{18}\text{O}$  and  $\delta\text{D}$  values of +9.3 to +14.2 ‰ and -65 to -31 ‰, respectively, which for the Sullivan deposit suggest tourmaline formation from mixtures of normal and exchanged seawater that had interacted with marine clastic sediments in the stratigraphic footwall sequence. The  $\delta^{18}\text{O}$  data for the shallow footwall tourmalinites at Sullivan show values 1 to 2 ‰ higher than those for the deep footwall tourmalinites, suggesting slightly different formational temperatures of ~230 to ~280 °C vs ~250 to ~300 °C, respectively (Seal et al. 2000). Calculated  $\delta^{18}\text{O}$  and  $\delta\text{D}$  data for the tourmaline-forming fluids further suggest an origin involving brines derived from evaporated seawater, followed by heating deep within the Belt–Purcell basin (Taylor et al. 2000).

## 5.2. Boron

Boron isotope data for tourmalines from inferred premetamorphic tourmalinites show a large variation from -26.1 to +27.5 ‰ (Fig. 8). This range of  $\delta^{11}\text{B}$  values approaches that for tourmaline from massive sulfide deposits (Palmer and Slack 1989) but does not reach the higher values of +20 to +35 ‰ reported for tourmaline from other types of hydrothermal ore deposits such as orogenic gold, iron oxide-copper-gold, and sediment-hosted uranium (Trumbull et al. 2020). Although the range of  $\delta^{11}\text{B}$  values for most natural reservoirs is relatively well known, problems still remain in identifying the predominant source of boron in tourmalinites as well as in tourmaline from various types of ore deposits. This is a particularly difficult challenge for isotopically light boron, for which tourmaline  $\delta^{11}\text{B}$  values in the range of -16 to -4 ‰ may reflect boron derived from several

sources, including granitic magmas, marine sediments, or non-marine evaporites and carbonates (Trumbull and Slack 2018; Trumbull et al. 2020). Other processes that may affect the boron isotopic composition of tourmaline include the temperature of formation, metamorphic fractionation, fluid/rock ratios, extent of seawater entrainment, and secular variation in seawater  $\delta^{11}\text{B}$  values (Palmer and Slack 1989). The boron source, however, is likely the predominant control.

Early studies proposed that  $\delta^{11}\text{B}$  values below ca. -18 ‰ in tourmalines reflect boron derived from non-marine evaporites (Palmer and Slack 1989; Slack et al. 1989; Palmer 1991). However, a more recent Li and B isotope study by Romer et al. (2014) of Cambrian shales in Germany reported  $\delta^{11}\text{B}$  values as low as -24.0 ‰, attributed to  $^{11}\text{B}$  depletion during intense weathering in the source terrane(s) of the shales. Therefore, such isotopically low values do not require a major boron contribution from non-marine evaporites, a model that also applies to tourmalinites that formed in this type of environment or had a boron source terrane that included sediments derived from a strongly weathered source. Consequently, a boron isotope range unique to non-marine evaporites (and related carbonates) cannot be robustly defined at present. This limitation is underpinned by recent proposals for very low boron isotope compositions of ancient seawater (Marschall 2018), including calculated values for Precambrian seawater of +14 to +26 ‰ (Chaussidon and Appel 1997; Grew et al. 2015; Ota et al. 2019) that are ca. 14 to 26 ‰ lower than the value of +39.5 ‰ documented for modern seawater. Available data for Archean and Paleoproterozoic tourmalinites (Broken Hill, Isua, Jervois) show  $\delta^{11}\text{B}$  values of  $\leq -20$  ‰ (Fig. 8), consistent with the hypothesis of isotopically light seawater boron existing during the early Precambrian, and possibly extending into the Paleozoic (Marschall 2018). However,  $\delta^{11}\text{B}$  values of -20.0 ‰ or lower for tourmaline are nonetheless consistent with a non-marine evaporite source, particularly in terranes where underlying strata are known to contain evaporites or metaevaporites, such as in the Broken Hill district where bedded albitites occur in the deep stratigraphic footwall to the Pb–Zn–Ag ores and to tourmalinites of the region (Slack et al. 1989, 1993).

Positive  $\delta^{11}\text{B}$  values, in contrast, can generally be assigned to a predominantly marine boron source (Fig. 8). More specifically, values higher than +10 ‰ likely reflect a source from marine carbonates and/or evaporites. Evidence for such sources comes from studies of tourmalinites hosted in metacarbonates and well-documented metaevaporites, including Mesoproterozoic strata in northwestern New York State that have tourmaline  $\delta^{11}\text{B}$  values of +10.5 ‰ (Palmer and Slack 1989), and Mesoproterozoic and Neoproterozoic strata in central and southern Namibia with tourmaline  $\delta^{11}\text{B}$  values of +18.3

and +12.0 to +27.5 ‰, respectively (Palmer and Slack 1989; Frimmel and Jiang 2001). Boron contained in these tourmalinites is believed to have originated via the leaching of boron from evaporites or carbonate rocks followed by upward transport in basinal brines to shallow depths on or below the seafloor. It is important to note, however, that carbonate rocks typically lack high concentrations of boron (<100 µg/g; Marschall 2018), hence such strata probably were not the sole boron source for tourmalinites except possibly thin units of limited stratigraphic extent. Isotopically heavy boron isotopes may also rule out non-marine evaporite origins previously inferred from geological and mineralogical data, as evidenced by the  $\delta^{11}\text{B}$  value of +18.3 ‰ for finely laminated Neoproterozoic tourmalinite at Stolzenfeld in central Namibia (Palmer and Slack 1989).

Many non-marine evaporites contain minor to abundant borate minerals (e.g., Helvacı and Palmer 2017) and hence are likely sources for the boron in abundant tourmalinites occurring in overlying strata. This hypothesis can be tested via mass-balance calculations for distinguishing between marine and non-marine sources of boron. For example, Slack et al. (2020) used this approach in evaluating the source of the ~52 Mt of boron contained within tourmalinite alteration zones of the Sullivan Pb–Zn–Ag orebody in Canada (Fig. 4). If the boron source for these tourmalinites was derived only from the underlying low-B (avg. 22.6 µg/g) clastic sediments, a very large sediment reservoir of 1733 km<sup>3</sup> is required. Including the volumetrically minor but widespread tourmalinites present in coeval strata of the Belt–Purcell Supergroup (Slack 1993) requires an even larger reservoir volume. In contrast, the leaching of deep (but unexposed) non-marine evaporitic borates needs a much smaller source volume of only 4 km<sup>3</sup>, assuming a borate deposit size of 200 Mt and an average grade of 13 wt. % B, based on data for the Boron and Kirka deposits in California and Turkey (Kistler and Helvacı 1994), together with an estimated 50% depositional efficiency for the tourmaline-hosted boron in the deposit. This non-marine evaporite source model is consistent with boron isotope data for ore-related tourmalinites from the Sullivan deposit ( $n = 57$ ) and for non-ore-related tourmalinites from the surrounding region ( $n = 21$ ), which overall show a range of –15.4 to –2.3 ‰ with averages of  $-8.4 \pm 2.3$  and  $-7.3 \pm 3.5$  ‰, respectively (Jiang et al. 1999, 2000a).

### 5.3. Silicon

Only a few silicon isotope studies have been done on tourmalinite-hosted tourmaline (Marschall and Jiang 2011). Results for tourmaline separates from tourmalinites in the Sullivan Pb–Zn–Ag deposit and in coeval metasedimentary strata of the surrounding Belt–Purcell

Supergroup range in  $\delta^{30}\text{Si}$  from –0.5 to 0.0 ‰; the unaltered host metasediments have values of 0.0 to +0.1 ‰ (Jiang et al. 1994, 2000b). The limited available data show that for the ore-related tourmalinites at Sullivan,  $\delta^{30}\text{Si}$  values lower than –0.1 ‰ are restricted to the shallow footwall, consistent with a major contribution of hydrothermal silicon to the tourmalinites in this part of the deposit. Because silicon isotope values of tourmaline (and other minerals) are not generally reset during metamorphism, such data may be useful as paleoenvironmental indicators and as stratigraphic guides for mineral exploration (Jiang 1998; Marschall and Jiang 2011).

Future studies that report  $\delta^{18}\text{O}$ ,  $\delta^{11}\text{B}$ ,  $\delta^{30}\text{Si}$ , and  $\delta\text{D}$  values for tourmalinite-hosted tourmaline could prove fruitful in better constraining the nature and origin of fluid sources involved in tourmalinite formation (Slack and Trumbull 2011; Cabral and Koglin 2012). Important advances will likely come from studies that integrate major-element data acquired by EMP with *in situ* analyses for trace elements by LA-ICP-MS and for boron isotopes by SIMS or other *in situ* techniques (e.g., Pesquera et al. 2005; Trumbull et al. 2008, 2011; Marschall and Jiang 2011; Su et al. 2016; Albert et al. 2018).

## 6. Discussion

### 6.1. Constraints on genesis

High alumina contents of tourmaline (ca. 28–35 wt. %  $\text{Al}_2\text{O}_3$ ) greatly limit plausible models of tourmalinite formation. The precipitation of tourmaline directly from an aqueous phase, such as metalliferous hydrothermal fluids, requires the transport of significant Al in solution. However, in hydrothermal fluids at low to moderate temperature (<300 °C), Al has appreciable solubility only under low (<5) or high (>8) pH values, or in those with high contents of fluoride, sulfate, or organic acids (Slack 1996 and references therein). In contrast, in high-temperature Si- and Cl-bearing metamorphic and magmatic fluids, Al solubility can be very high (up to ~80 mmol/kg; Manning 2006), thus explaining the presence of abundant tourmaline in such settings where fluid B concentrations were also high (e.g., Yardley 2013).

The minimum temperature of tourmaline stability is a further constraint. Although the lowest formational temperature in nature is unknown, a value below 150 °C has been proposed based on the occurrence of diagenetic tourmaline overgrowths in sandstones and authigenic grains in the cap rocks of a salt dome (Henry et al. 1999; Henry and Dutrow 2012). However, in modern seafloor-hydrothermal systems distal (>100 m) from vent sites, temperatures at or near the sediment-seawater interface are much lower, generally <50 °C (e.g., Humphris and

Tivey 2000). This low temperature and other considerations were the basis for past suggestions that tourmaline does not form directly in modern seafloor environments, instead being derived from an original B-rich gel or colloid precursor (Ethier and Campbell 1977; Slack et al. 1984; Slack 1996).

## 6.2. Seafloor processes of boron enrichment

The close spatial association of tourmalinites with many ancient VMS deposits provides compelling evidence for boron enrichment on the paleoseafloor during the formation of these deposits. Such tourmalinites may occur in the immediate footwall or hanging wall of the deposits, or as stratigraphic equivalents along strike (Fig. 1a). Occurrences of tourmalinites containing laminae of sphalerite and/or galena, as in the shallow footwall of the Sullivan Pb–Zn–Ag deposit (Slack et al. 2000b), support this seafloor depositional model for the initial concentration of boron. Also relevant are tourmalinites interlayered with coticles or those containing abundant spessartine-rich garnet (Fig. 2a, 3f), the latter manganese tourmalinites reflecting a Mn- and B-rich protolith that may have included minerals such as jimboite [ $\text{Mn}_3\text{B}_2\text{O}_6$ ] and sussexite [ $\text{MnBO}_2(\text{OH})$ ], which occur in some bedded Mn ores (Epprecht et al. 1959; Kato and Matsubara 1980). The manganese within these tourmalinites and related coticles was likely deposited from proximal or distal, non-buoyant hydrothermal plumes that were dispersed in seawater over large areas (tens to thousands of  $\text{km}^2$ ), based on data for Mn-rich metalliferous sediments in the modern Red Sea and the eastern Pacific Ocean (e.g., Barrett et al. 2021). This interpretation is supported by the presence of high boron concentrations in eastern Pacific Ocean sediments that include values of up to 830  $\mu\text{g/g}$  B (Boström and Peterson 1969) and by the areal distribution of modern Mn- and Fe-rich hydrothermal plumes that extend up to 4300 km westward from the East Pacific Rise (Fitzsimmons et al. 2017). Tourmalinite-coticle units in terranes that lack known VMS or other stratabound mineralization probably formed by similar volcanic-hydrothermal processes and may be useful in the field as stratigraphic markers (Kennan and Kennedy 1983; Slack 1996).

Aluminum contents in vent fluids of modern seafloor-hydrothermal systems are very low (<0.02 mmol/kg; German and Von Damm 2003) and hence are insufficient to permit tourmaline saturation and subsequent direct precipitation of this mineral on the seafloor. Moreover, these vent fluids are rapidly diluted by mixing with ambient seawater (Elderfield et al. 1993) and related plume particles have extremely low Al contents ( $\leq 12$  nmol/L; Feely et al. 1994). Another major limitation is that molar Fe/Al ratios in modern submarine-hydrothermal fluids

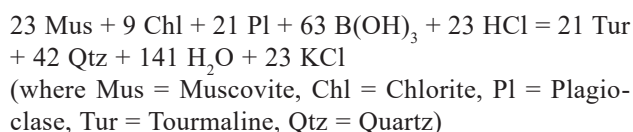
are very high ( $\sim 10$ –300; German and Von Damm 2003) and are extremely high in plume particles (avg. 4663; Feely et al. 1994), whereas the ratios in tourmaline from tourmalinites are much lower ( $\sim 1$ –6; Slack et al. 1993; Jiang et al. 1998; Pesquera et al. 2005; Čopjaková et al. 2009). Hence, any exhalative submarine-hydrothermal fluid that precipitated tourmaline would consume so much Al initially that the fluids would be undersaturated with respect to tourmaline away from the vent sites, and thus be incapable of forming laterally extensive syngenetic tourmalinites (Slack 1996). Collectively, these data provide compelling arguments against a model for stratiform tourmalinite formation in which the tourmaline was a direct precipitate, on the seafloor, from submarine-hydrothermal fluids.

Previous workers have speculated that B-rich gels or colloids were protoliths to premetamorphic tourmalinites, including those in or near VMS and CD Pb–Zn deposits (e.g., Ethier and Campbell 1977; Slack et al. 1984; Jiang et al. 1994; Ndiaye and Guillou 1997). Possible support for this hypothesis comes from the presence of small (<1 cm) spheroidal structures within shallow footwall tourmalinites at the Sullivan Pb–Zn–Ag deposit (Slack et al. 2000b) that are like those produced experimentally in dehydrated siliceous gels (Oehler 1976). Similar globular structures <1 cm in size were reported in tourmalinites from Senegal and Mali by Ndiaye and Guillou (1997). Importantly, however, no evidence exists in modern seafloor-hydrothermal systems for B-rich phases. Yet textural evidence strongly suggests this type of origin for the Si–Fe and Mn-rich beds in early Paleozoic VMS deposits of Norway and Spain (Grenne and Slack 2003a; Jorge et al. 2005), and in modern plume particles and metalliferous sediments on the Juan de Fuca Ridge and in the Red Sea, respectively (Hrischeva and Scott 2007; Laurila et al. 2015). A challenge for future studies will be proving the existence of B-rich gels or colloids in modern seafloor-hydrothermal systems.

## 6.3. Syngenetic and diagenetic boron metasomatism

The critical role of precursor aluminous sediments or felsic volcanic rocks during the formation of stratiform tourmalinites supports a diagenetic origin involving B-rich hydrothermal fluids. This model is consistent with numerous observations of tourmalinites that preserve sedimentary structures such as graded beds, cross-laminations, and rip-up clasts (Slack et al. 1984; Slack 1996). Within these structures, tourmaline shows preferential replacement of the clay and/or feldspar matrix. A preferred origin (Slack 1993, 1996) involves the migration of B-rich hydrothermal fluids along permeable, sandy beds and the selective replacement of argillaceous

beds (or laminae) in the upper parts of unconsolidated sedimentary sequences. This replacement process may occur at or near the sediment-water interface, or tens to hundreds of meters below. Such a model is also applicable to permeable felsic volcanics, especially aluminous volcaniclastic rocks (Bandyopadhyay et al. 1993). Rarely, basalt may be the locus of boron metasomatism and tourmaline formation, as at the Elizabeth VMS deposit in Vermont (Slack et al. 2001), although in this case, the tourmalinite formed by extreme metasomatic processes. The timing of replacement most likely was during sedimentation or early diagenesis, involving episodic basin dewatering (Slack 1996) and the release of boron from illite during the 1Md-2M<sub>1</sub> transition (Reynolds 1965), with the subsequent focusing of B-rich fluids preferentially in synsedimentary fault zones (cf. Bjørlykke 2015). A much later timing (e.g., metamorphic) is also possible if sufficient permeability is maintained for fluid transport over large distances (> 100 m) within individual beds or laminae. Regardless of the timing, for typical precursor mineral assemblages, a generalized reaction can be written as follows (Slack 1996):



This reaction produces quartz as a product, consistent with the presence in some tourmalinites of hydrothermal quartz intergrown with tourmaline (e.g., Jiang et al. 1998) and of quartz-rich selvages along margins of tourmalinites (Slack 1996). However, the quartz in many tourmalinite-hosted tourmalines may also derive from Si-rich hydrothermal fluids, as suggested by the low silicon isotope values of tourmalinites in the Sullivan Pb–Zn–Ag deposit (Jiang et al. 1994, 2000b).

Boron metasomatism of aluminous sediments under high fluid/rock conditions can greatly affect concentrations of alkali and alkaline earth elements and LREE, as discussed above for the footwall tourmalinite pipe at the Sullivan Pb–Zn–Ag deposit. The major variations in LREE abundances evident for the shallow footwall tourmalinites (Fig. 6a) and for some deep footwall tourmalinites (Slack et al. 2000b) suggest local dissolution and reprecipitation of detrital monazite and of other LREE-rich detrital phases such as allanite. However, this hypothesis has not been tested and is a worthwhile project at Sullivan and elsewhere, focusing on microtextural and microchemical data obtained by EMPA, scanning electron microscopy (SEM), and LA-ICP-MS.

The formation of tourmalinites in some terranes likely reflects boron recycling processes. An early stage involves the dissolution of B-bearing phases, especially clays that may contain as much as 2000 µg/g B (Harder 1970), and the transfer of this boron by hydrothermal

fluids towards the paleoseafloor. Later stages can include preexisting tourmaline concentrations that during metamorphism, are remobilized into veins and metasomatic replacements, or during granite emplacement, are incorporated into the magma and subsequently crystallize as tourmaline-rich pegmatites, nodules, and veins (e.g., Slack et al. 1993; Slack 1996; Kasemann et al. 2000; Pesquera et al. 2005; Krmíček et al. 2021). The predominance of tourmalinites in the Proterozoic (Tab. 1) also suggests the possibility that coeval seawater had higher boron contents than today, thus favoring the formation of tourmaline-rich sediments during sedimentation and early diagenesis of that Eon.

#### 6.4. Potential modern analogs

Modern analogs of tourmalinites are unknown. However, in seafloor environments, limited data suggest there is a general affinity of B with Mn, as for sediments on the East Pacific Rise that contain 300 to 800 µg/g B (carbonate-free basis) associated with Al-poor Fe–Mn sediments (Boström and Peterson 1969). In this setting, B-rich precursors to tourmaline may exist, a possibility supported by the finely interbedded nature of tourmalinites and cotecules in numerous metasedimentary and metavolcanic terranes worldwide (Slack et al. 1984; Spry et al. 2000). A related constraint is the low B concentration expected in non-buoyant hydrothermal plumes distal from seafloor vent sites, owing to the large dilution factor (~10<sup>4</sup>) for vent fluids during mixing with ambient seawater, as calculated for modern plumes (German and Von Damm 2003). Overall, among tourmalinites that formed at or near the seafloor, many have sources and contained components of (1) hydrothermal plumes: Fe, Mn, Si, B; (2) sediments and felsic volcanics: B, Al, Si, Mg, Ca, Na; (3) evaporites: B, Mg; and (4) seawater: B, Mg, and Si; the last component is restricted to pre-Cretaceous tourmalinites because of very low Si contents of seawater thereafter, due to the rise of diatoms and other siliceous organisms (Grenne and Slack 2003b). In evaporitic settings, tourmaline precursors may have included mixtures of a detrital ferromagnesian silicate, like chlorite with Na ± Ca borosilicates such as reedmergnerite [NaBSi<sub>3</sub>O<sub>8</sub>] or searlesite [NaBSi<sub>2</sub>O<sub>5</sub>(OH)<sub>2</sub>], both of which are locally abundant in Tertiary lacustrine evaporite deposits of the western United States (Milton 1971).

A second potential seafloor site for modern B-rich sediments is at or near high-temperature hydrothermal systems hosted in aluminous sediments or felsic volcanic rocks. Whereas modern, sediment-free (basaltic) systems have vent fluids with ca. 350 to 700 µmol/kg B, those of sediment and rhyolite systems have much higher B concentrations up to 4800 µmol/kg (Yamaoka et al. 2015); for comparison, seawater has an average of 415 µmol/

kg B (German and Von Damm 2003). The combination of high B within these vent fluids, and the availability of abundant Al in the host sediments and felsic volcanics, suggests potential in such environments for modern tourmalinite formation. This potential most likely exists in the subsurface where seawater dilution of B-rich hydrothermal fluids is generally minimized.

The Red Sea has several features that suggest the possible modern formation of B-rich phases. Metaliferous brines in the various basins have temperatures up to 68 °C and boron concentrations up to 4580 µmol/kg in the Oceanographer Deep (Schmidt et al. 2015). Interstitial waters in the Atlantis II Deep contain up to 880 µmol/kg (Anschutz et al. 2000), and ca. 1000 µg/g B was determined for two Fe- and Zn-rich samples from shallow core depths of 15 to 25 cm in the Atlantis II Deep (Hendricks et al. 1969). A more comprehensive study by Laurila et al. (2014) found much lower maximum boron contents of 120 µg/g B in sediments from the Atlantis II Deep. Importantly, a moderate correlation ( $r = 0.61$ ) of B with sulfide sulfur determined in that study suggests that the boron preferentially occurs in Fe-sulfide-facies metalliferous sediment and not the Fe- and Mn-oxide-facies sediment that predominates in the Red Sea deposits. Unknown is whether some of the basins there or geographic or stratigraphic parts of the basins, contain B-rich brines and sediments whereas others do not. Notably, the relatively high boron concentrations within the Red Sea brines may still be too low for tourmaline growth on the underlying seafloor, given the nucleation barrier that exists for this mineral at low temperatures of ca. 150 °C or less (Henry and Dutrow 2012). Although tourmaline precipitation is unlikely in surficial sediments of the Red Sea, tourmaline could be forming in the subsurface at higher temperatures, at or near hydrothermal conduits like those documented in the Atlantis II Deep (150–420 °C; Zierenberg and Shanks 1983, 1988), or via the heating of B-rich pore fluids by mafic intrusions such as the gabbro bodies identified recently in the Discovery Deep (Follmann et al. 2021). Alternatively, downward penetration of the dense B-rich brines into sediments in the shallow subsurface (cf. Sangster 2002) might be forming amorphous B-rich phases (gels, colloids).

A final potential setting for the formation of modern tourmalinites is near the margins of large mafic sills or dikes that intrude marine clastic sediments. This hypothesis is based on the analogy with the setting of tourmalinites in some Proterozoic sedimentary basins such as the Belt-Purcell Supergroup, in which tourmalinites (and local albitites) occur near the margins of large gabbroic sills that were emplaced while the host sediments were still un lithified (Beatty et al. 1988; Höy et al. 2000). Occurrences of these types of synsedimentary mafic sills are well documented in modern sedimentary basins as

in parts of the Norwegian Sea and the South China Sea (Jamtveit et al. 2004; Zhao et al. 2021). A reconnaissance study of a drill core through a dolerite sill in the Guaymas Basin, Gulf of California, indicates that during emplacement of this sill, the boron in surrounding clastic sediments was remobilized and concentrated in the margins of the sill, by a factor of ca. 50, producing vented hydrothermal fluids with boron contents of up to 1730 µmol/kg relative to the seawater value of 415 µmol/kg B (Spivack et al. 1987). This mafic sill heated the adjacent sediments to temperatures of ~250 to 350 °C based on oxygen isotopes (e.g., Kastner 1982). Therefore if boron concentrations are sufficiently high, then tourmalinite occurrences are possible, not only in Guaymas Basin but in other modern sill-sediment complexes that also may have associated clastic-hosted Pb–Zn–Ag deposits (Slack 2020).

### 6.5. Exploration applications

A first-order exploration guide in premetamorphic stratabound tourmalinites is the presence of base-metal sulfide minerals, including discrete grains and tourmaline-hosted inclusions. The occurrence of an accessory or minor pyrite or pyrrhotite alone may not be prospective. On a whole-rock basis, tourmalinites with high MnO contents (>1 wt. %) present in carbonate or garnet (Fig. 3f) are interpreted to have an appreciable exhalative hydrothermal component and thus possibly be time-correlative with stratiform sulfide mineralization along strike (Slack 1996). The presence of povondraite-rich tourmaline, containing high proportions of Fe<sup>3+</sup>, likely reflects deposition from high-salinity fluids (Henry et al. 2008), and hence settings in which abundant base metals could be transported (e.g., Zhong et al. 2015). Dravite and other Mg-rich tourmalines may be informative, especially where associated with sulfide minerals even in small amounts of ca. 1 vol. %, because such magnesian compositions can record the involvement of evolved (Mg-rich) seawater in seafloor-hydrothermal systems and the effects of sulfide-silicate reactions during metamorphism (Slack 1996). However, Mg-rich tourmaline also occurs in many barren tourmalinites that lack any relationship to base-metal or other metallic mineralization, instead reflecting formational conditions under low fluid/rock ratios in which the bulk composition of magnesian host rocks (e.g., evaporitic sediments) controlled tourmaline chemistry (Slack 1996; Pesquera et al. 2005).

Data for REE can also be useful in mineral exploration programs. Positive Eu anomalies are especially valuable in recording deposition from reduced, high-temperature fluids that can transport metals of economic interest (e.g., Lottermoser 1992; Slack 1996). However, tourmalinites that lack such anomalies may not be favorable explo-

ration guides, instead reflecting processes such as the diagenetic mobilization and venting of B-rich, but metal-poor basinal fluids. An important caveat in this context is that tourmalinites without positive Eu anomalies may still have associated mineralization since many ore-related tourmalines in the Broken Hill district do not show these anomalies (Fig. 6b).

### 6.6. Archean tourmalinites and early life

Ribonucleic acid (RNA) is generally considered a fundamental precursor of deoxyribonucleic acid (DNA) and hence a molecule critical for the origin of life (e.g., Neveu et al. 2013). A major requirement for the evolution of RNA is ensuring its stability within ribose at circumneutral pH, a problem that may be solved by the presence of borate compounds (Grew et al. 2011). Therefore, occurrences of boron-rich minerals in the early rock record of Earth are potentially important for paleobiology. A related issue is a geological environment where life originated, which is a highly controversial topic that is widely debated. A major advance comes from the study of Weiss et al. (2016), which involved a detailed assessment of phylogenetic trees for 6.1 million protein-coding genes, the results suggesting that the last universal common ancestor (LUCA) lived in a hydrothermal environment containing high concentrations of Fe, S, H<sub>2</sub>, and CO<sub>2</sub>. This environment is consistent with a seafloor setting related to submarine volcanism and hot springs. Byerly et al. (1986) first alluded to the role that tourmalinites may play in early life, based on the presence of tourmaline-rich laminae within stromatolites of the Paleoarchean Barberton greenstone belt in South Africa. This hypothesis of a link between tourmalinites and early life was also evaluated for tourmalinites of the Eoarchean Isua supracrustal belt of West Greenland by Grew et al. (2015). More recent discussions of this concept, as applied to the Isua tourmalinites and those of Mesoarchean age, are presented in Mishima et al. (2016), Ota et al. (2019), and Van Kranendonk et al. (2021). However, fundamental geological constraints for the borate-RNA model are that no borate minerals are known in such ancient rocks and that the isotopically very low  $\delta^{11}\text{B}$  values of the tourmalinite-hosted tourmalines ( $-25.0$  to  $-17.3$  ‰; Chaussidon and Appel 1997) are not proof of a non-marine evaporite origin for the boron, given the likelihood that Early Archean seawater had much lower  $\delta^{11}\text{B}$  values than today (e.g., Grew et al. 2015). Moreover, if life began not in the Eoarchean (ca. 3.8–3.7 Ga) as currently envisaged but instead in the Hadean (Martin et al. 2008), then the lack of rocks older than 4 Ga, including those with tourmaline (Grew et al. 2011) is an additional limitation for a connection of borate compounds to the emergence of RNA on primordial Earth.

*Acknowledgments:* This paper relies on four decades of tourmalinite field work and research collaboration with numerous colleagues. In particular, I wish to thank Doug Anderson, Frickie Badenhorst, Rob Barnes, Jim Finch, Bill Griffin, Greg Hahn, Darrell Henry, Neil Herriman, Trygve Höy, Shao-Yong Jiang, Padhraig Kennan, Craig Leitch, Peter Nicholson, Martin Palmer, Alfonso Pesquera, Ian Plimer, Hubertus Porada, Paul Ransom, Barney Stevens, Bruce Taylor, Bob Trumbull, and Bob Turner for field guidance, stable isotope analyses, and discussions. Appreciation is also extended to the management and geological staff of the many exploration and mining companies worldwide, who provided me with invaluable access to properties, mines, and drill cores for study. The thorough reviews of Shao-Yong Jiang, Ryan McAleer, Alfonso Pesquera, and Guest Editor Horst Marschall improved the manuscript. Any use of trade, firm, or product names is for descriptive purposes only and does not imply endorsement by the U.S. Government.

### References

- ABRAHAM K, MIELKE H, POVONDRA P (1972) On the enrichment of tourmaline in metamorphic sediments of the Arzberg Series, West Germany (NE Bavaria). *Neu Jb Mineral, Mh* 5: 209–219
- ABRAMS CE, MCCONNELL KI (1984) Geologic setting of volcanogenic base and precious metal deposits of the west Georgia Piedmont: a multiply deformed metavolcanic terrain. *Econ Geol* 79: 1521–1539
- ALBERT C, LANA C, GERDES A, SCHANNOR M, NARDUZZI F, QUEIROGA G (2018) Archean magmatic-hydrothermal fluid evolution in the Quadrilátero Ferrífero (SE Brazil) documented by B isotopes (LA MC-ICPMS) in tourmaline. *Chem Geol* 481: 95–109
- ANSCHUTZ P, BLANC G, MONNIN C, BOULÈGUE J (2000) Geochemical dynamics of the Atlantis II Deep (Red Sea): II. Composition of metalliferous sediment pore waters. *Geochim Cosmochim Acta* 64: 3995–4006
- APPEL PWU (1985) Strata-bound tourmaline in the Archean Malene supracrustal belt, West Greenland. *Can J Earth Sci* 22: 1485–1491
- APPEL PWU (1988a) Stratiform tourmalinites in the Archean tungsten province of West Greenland. *Mineral Petrol* 39: 79–91
- APPEL PWU (1988b) Tourmaline in Precambrian supracrustal rocks from Aasiaat, central West Greenland. *Rapp Grønlands Geol Undersøg* 140: 44–46
- APPEL PWU (1992) Tourmalinites in supracrustal rocks in the Bjørnesund area, West Greenland. *Rapp Grønland Geol Unders* 155: 73–78
- APPEL PWU (1995) Tourmalinites in the 3800 Ma old Isua supracrustal belt, West Greenland. *Precamb Res* 72: 227–234

- APPEL PWU, GARDE AA (1987) Stratabound scheelite and stratiform tourmalinites in the Archaean Malene supracrustal rocks, southern West Greenland. *Grønland Geol Unders Bull* 156: 1–26
- ARENA KR, HARTMANN LA, LANA C, QUEIROGA GN, CASTRO MP (2020) Geochemistry and  $^{11}\text{B}$  evolution of tourmaline from tourmalinite as a record of oceanic crust in the Tonian Ibaré ophiolite, southern Brasiliano orogen. *An Acad Bras Cienc* 92, DOI: 10.1590/0001-3765202020180193
- ARRIBAS-ROSADO A (1986) The significance of tourmaline in stratabound tungsten deposits in Spain. *Tungsten Deposits Conference*, Toulouse, France. Abstract Volume, p 33
- BADENHORST FP (1988) A note on stratiform tourmalinites in the late Precambrian Kuiseb Formation, Damara sequence. *Commun Geol Survey SW Africa/Namibia* 4: 77–80
- BANDYOPADHYAY BK, SLACK JF, PALMER MR, ROY A (1993) Tourmalinites associated with stratabound massive sulfide deposits in the Proterozoic Sakoli Group, Nagpur district, central India. In: Maurice YT (ed) *Proceed Eighth Quad IAGOD Symp*, Ottawa, Canada. E. Schweizerbart'sche Verlagsbuchhandlung, Stuttgart, Germany, pp 867–885
- BARNES RG (1983) Stratiform and stratabound tungsten mineralization in the Broken Hill Block, N.S.W. *J Geol Soc Aust* 30: 225–239
- BARNES RG (1988) Metallogenic studies of the Broken Hill and Euriovie blocks, New South Wales. 1. Styles of mineralization in the Broken Hill block. *New South Wales Geol Survey Bull* 32(1): 1–115
- BARRETT TJ, JARVIS I, HANNINGTON MD, THIRLWALL MF (2021) Chemical characteristics of modern deep-sea metalliferous sediments in closed versus open basins, with emphasis on rare-earth elements and Nd isotopes. *Earth-Sci Rev* 222, <https://doi.org/10.1016/j.earsci-rev.2021.103801>
- BEATY DW, HAHN GA, THRELKELD WE (1988) Field, isotopic, and chemical studies of tourmaline-bearing rocks in the Belt-Purcell Supergroup: genetic constraints and exploration significance for Sullivan-type ore deposits. *Can J Earth Sci* 25: 392–402
- BEHR H-J, AHRENDT H, MARTIN H, PORADA H, ROHRS J, WEBER K (1983) Sedimentology and mineralogy of Upper Proterozoic playa-lake deposits in the Damara orogen. In: MARTIN H, EDER FW (eds) *Intracontinental fold belts*. Springer-Verlag, Berlin-Heidelberg, pp 577–610
- BENVENUTI M, LATTANZI P, TANELLI G (1989) Tourmalinite-associated Pb–Zn–Ag mineralization at Bottino, Apuane Alps, Italy: geologic setting, mineral textures, and sulfide chemistry. *Econ Geol* 84: 1277–1292
- BENVENUTI M, COSTAGLIOLA P, LATTANZI P, TANELLI G (1991) Mineral chemistry of tourmalines from the Bottino mining district, Apuane Alps (Italy). *Eur J Mineral* 3: 537–548
- BERNIER L, POULIOT G, MACLEAN WH (1987) Geology and metamorphism of the Montauban north gold zone: a metamorphosed polymetallic exhalative deposit, Grenville Province, Quebec. *Econ Geol* 82: 2076–2090
- BJØRLYKKE K (2015) Subsurface water and fluid flow in sedimentary basins. In: Bjørlykke K (ed) *Petroleum geoscience: from sedimentary environments to rock physics*. Springer, Berlin-Heidelberg, pp 279–300
- BOERBOOM TJ (1989) Tourmaline in Early Proterozoic metasedimentary rocks near Philbrook, northeastern Todd County, central Minnesota. *Minnesota Geol Survey Rept Invest* 38, 25 p
- BONE Y (1988) The geological setting of tourmalinite at Rum Jungle, N.T., Australia – genetic and economic implications. *Miner Depos* 23: 34–41
- BOOKSTROM AA, BOX SE, COSSETTE PM, FROST TP, GILLERMAN VS, KING GR, ZIRAKPARVAR NA (2016) Geologic history of the Blackbird Co–Cu district in the Lemhi sub-basin of the Belt-Purcell basin. In: MACLEAN JS, SEARS JW (eds) *Belt basin: window to Mesoproterozoic Earth*. *Geol Soc Am, Spec Paper* 522, pp 185–219
- BOSTRÖM K, PETERSON MNA (1969) The origin of aluminum-poor ferromanganous sediments in areas of high heat flow on the East Pacific Rise. *Marine Geol* 7: 427–447
- BOZKURT E, WINCHESTER JA, MITTWEDE SK, OTTLEY CJ (2006) Geochemistry and tectonic implications of leucogranites and tourmalines of the southern Menderes massif, southwest Turkey. *Geodin Acta* 19: 363–390
- BROWN CE, AYUSO RA (1985) Significance of tourmaline-rich rocks in the Grenville Complex of St. Lawrence County, New York. *US Geol Survey Bull* 1626–C, 33 p
- BYERLY GR, PALMER MR (1991) Tourmaline mineralization in the Barberton greenstone belt, South Africa: Early Archean metasomatism by evaporite-derived boron. *Contrib Mineral Petrol* 107: 387–402
- BYERLY GR, LOWE DR, WALSH MM (1986) Stromatolites from the 3,300–3,500-Myr Swaziland Supergroup, Barberton mountain land, South Africa. *Nature* 319: 489–491
- CABRAL AR, KOGLIN N (2012) Hydrothermal fluid source constrained by Co/Ni ratios in coexisting arsenopyrite and tourmaline: the auriferous lode of Passagem, Quadrilátero Ferrífero of Minas Gerais, Brazil. *Mineral Petrol* 104: 137–145
- CABRAL AR, LEHMANN B, TUPINAMBÁ M, WIEDENBECK M, BRAUNS M (2011) Geology, mineral chemistry and tourmaline B isotopes of the Córrego Bom Sucesso area, southern Serra do Espinhaço, Minas Gerais, Brazil: implications for Au–Pd–Pt exploration in quartzitic terrain. *J Geochem Explor* 110: 260–277
- CHAUSSIDON M, APPEL PWU (1997) Boron isotopic composition of tourmalines from the 3.8-Ga-old Isua supracrustals, West Greenland: implications on the  $\delta^{11}\text{B}$  value of Early Archean seawater. *Chem Geol* 136: 171–180

- CHOWN EH (1987) Tourmalinites in the Apehebian Mistassini Group, Quebec. *Can J Earth Sci* 24: 826–830
- CLELAND JM, MOREY GB, MCSWIGGEN PL (1996) Significance of tourmaline-rich rocks in the North Range Group of the Cuyuna Iron Range, east-central Minnesota. *Econ Geol* 91: 1282–1291
- COLLAO S, ALFARO G, HAYASHI K (1990) Banded iron formation and massive sulfide ore bodies, south-central Chile: geological and isotopic aspects. In: FONTBOTÉ L, AMSTUTZ GC, CARDOZO M, CEDILLO E, FRUTOS J (eds) *Stratabound ore deposits in the Andes*. Springer, Heidelberg, pp 209–219
- CONWAY CM (1986) Field guide to Early Proterozoic strata that host massive sulfide deposits at Bagdad, Arizona. In: NATIONS JD, CONWAY CM, SWANN GA (eds) *Geology of central and northern Arizona*. *Geol Soc Am Guidebook (Rocky Mtn Sect)*, pp 104–157
- ČOPJAKOVÁ R, BURIÁNEK D, ŠKODA R, HOUZAR S (2009) Tourmalinites in the metamorphic complex of Svratka unit (Bohemian massif): a study of compositional growth of tourmaline and genetic relations. *J Geosci* 54: 221–243
- ČOPJAKOVÁ R, ŠKODA R, NOVÁK M, VAŠINOVÁ GALIOVÁ M (2013) Geochemistry of Y+REE in stratiform tourmalinites and their tourmalines: implications for their genesis. In: JONSSON E et al. (eds) *Mineral deposit research for a high-tech world*. *Geol Survey Sweden, Uppsala, Proceed 12<sup>th</sup> Bienn SGA Mtg, vol. 4*, pp 1705–1708
- CROWLEY JK (1996) Mg- and K-bearing borates and associated evaporites at Eagle Borax Spring, Death Valley, California: a spectroscopic exploration. *Econ Geol* 91: 622–635
- CUNNINGHAM WB, HÖLL R, TAUPITZ KC (1973) Two new tungsten bearing horizons in the older Precambrium [sic] of Rhodesia. *Miner Depos* 8: 200–203
- DE BRODTKORB MK, PEZZUTTI N, BRODTKORB A, SCHIDLOWSKY M (1985) Tourmaline-schists and their relationship to Precambrian scheelite deposits from the San Luis province, Argentina. *Monogr Series Min Deposits*. Gebrüder Bornträger, Berlin, 25, pp 151–160
- DOMMANGET A, MILÉSI JP, DIALLE M (1993) The Loulo gold and tourmaline-bearing deposit. *Miner Depos* 28: 253–263
- D’ORAZIO M, BIAGIONI C, DINI A, VEZZONI S (2017) Thallium-rich pyrite ores from the Apuan Alps, Tuscany, Italy: constraints for their origin and environmental concerns. *Miner Depos* 52: 687–707
- ELDERFIELD H, GREAVES MJ, RUDNICKI MD, HYDES DJ (1993) Aluminum reactivity in hydrothermal plumes at the Mid-Atlantic Ridge. *J Geophys Res* 98(B6): 9667–9670
- EPPRECHT WT, SCHALLER WT, VLISIDIS AC (1959) Über Wiserit, Sussexit, und ein weiteres Mineral aus den Manganezen vom Gonzen (bei Sargans). *Schweiz Mineral Petrogr Mitt* 39: 85–104
- ETHIER VG, CAMPBELL FA (1977) Tourmaline concentrations in Proterozoic sediments of the southern Cordillera of Canada and their economic significance. *Can J Earth Sci* 14: 2348–2363
- FARBER K, DZIGGEL A, TRUMBULL RB, MEYER FM, WIENDENBECK M (2015) Tourmaline B-isotopes as tracers of fluid sources in silicified Palaeoarchean oceanic crust of the Mendon Formation, Barberton greenstone belt, South Africa. *Chem Geol* 417: 134–147
- FEELY RA, GENDRON JF, BAKER ET, LEBON GT (1994) Hydrothermal plumes along the East Pacific Rise, 8°40’ to 11°50’ N: particle distribution and composition. *Earth Planet Sci Lett* 128: 19–36
- FERLA P, MELI C (2007) Petrogenesis of tourmaline rocks associated with Fe-carbonate-graphite metapelite, metabasite and strata-bound polymetallic sulfide mineralisation, Peloritani Mountains, Sicily, southern Italy. *Lithos* 99: 266–288
- FERNÁNDEZ A, MORO MC (1992) Las turmalinitas estratiformes Ordovícicas de latado en el flanco s del sinforme de Alcañices (Zamora). *Estudios Geol* 48: 31–41
- FITZSIMMONS JN, JOHN SG, MARSAY CM, HOFFMAN CL, NICHOLAS SL, TONER BM, GERMAN CR, SHERRELL RM (2017) Iron persistence in a distal hydrothermal plume supported by dissolved-particulate exchange. *Nat Geosci* 10: 195–201
- FLEISCHER R, ROUTHIER P (1973) The “consanguineous” origin of a tourmaline-bearing gold deposit: Passagem de Mariana (Brazil). *Econ Geol* 68: 11–22
- FOLLMANN J, VAN DER ZWAN FM, PREINE J, HÜBSCHER C, BOUSQUET R, AUGUSTIN N (2021) Gabbro discovery in Discovery Deep: first plutonic rock samples from the Red Sea rift axis. *Frontiers Earth Sci* 9, doi 10.3389/feart.2021.742815
- FRANZ G, KUTZSCHBACH M, BERRYMAN EJ, MEIXNER A, LOGES A, SCHULTZE D (2021) Geochemistry and paleogeographic implications of Permo-Triassic metasedimentary cover from the Tauern Window (Eastern Alps). *Eur J Mineral* 33: 401–423
- FRIETSCH R (1991) New ore types in the northern part of the Fennoscandian Shield. *Geol Fören Förh* 113: 46–48
- FRIMMEL HE, JIANG S-Y (2001) Marine evaporites from an oceanic island in the Neoproterozoic Adamastor ocean. *Precambr Res* 105: 57–71
- GALLEY AG, HANNINGTON MD, JONASSON IR (2007) Volcanogenic massive sulfide deposits. In: Goodfellow WD (ed) *Mineral deposits of Canada: a synthesis of major deposit-types, district metallogeny, the evolution of geological provinces, and exploration methods*. *Geol Assoc Canada, Min Deposits, Div Spec Publ* 5, pp 141–161
- GARDA GM, BELJAVSKIS P, D’AGOSTINO LZ, WIENDENBECK M (2010) Tourmaline and rutile as indicators of a magmatic-hydrothermal origin for tourmalinite layers in the São José do Barreiro area, NE Ribeira belt, southern Brazil. *Rev Inst Geoci* 10: 97–117

- GARDA GM, BRENTAN F, BASEI MAS (2013) Tourmalinites of the Brusque Group in the São João Batista-Tijucas area, State of Santa Catarina, Brazil. *Rev Inst Geoci USP* 13: 73–94
- GERMAN CR, VON DAMM KL (2003) Hydrothermal processes. In: ELDERFIELD H (ed) *The oceans and marine geochemistry*. Elsevier, Amsterdam, *Treatise on Geochemistry* 6, pp 181–222
- GOLANI PR, PANDIT MK, SIAL AN, FALLICK AE, FERREIRA VP, ROY AB (2002) B–Na rich Palaeoproterozoic Aravalli metasediments of evaporitic association, NW India: a new repository of gold mineralization. *Precambr Res* 116: 183–198
- GRENE T, SLACK JF (2003a) Bedded jaspers of the Ordovician Løkken ophiolite, Norway: seafloor deposition and diagenetic maturation of hydrothermal plume-derived silica-iron gels. *Miner Depos* 38: 625–639
- GRENE T, SLACK JF (2003b) Paleozoic and Mesozoic silica-rich seawater: evidence from hematitic chert (jasper) deposits. *Geology* 31: 319–322
- GREW ES, BADA JL, HAZEN RM (2011) Borate minerals and origin of the RNA world. *Origin Life Evol Biosphere* 41: 307–316
- GREW ES, CARSON CJ, CHRISTY AG, BOGER SD (2013) Boron- and phosphate-rich rocks in the Larsemann Hills, Prydz Bay, East Antarctica: tectonic implications. In: HARLEY SL, FITZSIMONS ICW, ZHAO Y (eds) *Antarctica and supercontinent evolution*. *Geol Soc London Spec Publ* 383, pp 73–94
- GREW ES, DYMEK RF, DE HOOG JCM, HARLEY SL, BOAK J, HAZEN RM, YATES MG (2015) Boron isotopes in tourmaline from the 3.7–3.8 Ga Isua supracrustal belt, Greenland: sources for boron in Eoarchean continental crust and seawater. *Geochim Cosmochim Acta* 163: 156–177
- GRIFFIN WL, SLACK JF, RAMSDEN AR, WIN TT, RYAN CG (1996) Trace elements in tourmalines from massive sulfide deposits and tourmalinites: geochemical controls and exploration applications. *Econ Geol* 91: 657–675
- HANNINGTON MD (2014) Volcanogenic massive sulfide deposits. In: SCOTT SD (ed) *Geochemistry of mineral deposits*. Elsevier, Amsterdam, *Treatise on Geochemistry*, 2<sup>nd</sup> Ed, 7, pp 463–488
- HARDER H (1970) Boron content of sediments as a tool in facies analysis. *Sed Geol* 4: 153–175
- HELLINGWERF RH, LILLJEQUIST R, LJUN S (1988) Stratiform Zn–Pb–Fe–Mn mineralization in the Älvlänge-Vikern area, Bergslagen, Sweden. *Geol Mijnbouw* 2–4: 313–332
- HELLINGWERF RH, GATEDAL K, GALLAGHER V, BAKER JH (1994) Tourmaline in the central Swedish ore district. *Miner Depos* 29: 189–205
- HELVACI C, ORTÍ F (2004) Zoning in the Kirka borate deposit, western Turkey: primary evaporitic fractionation or diagenetic modifications? *Canad Mineral* 42: 1179–1204
- HELVACI C, PALMER MR (2017) Origin and distribution of evaporite borates: the primary economic sources of boron. *Elements* 13: 249–254
- HENDRICKS RL, REISBICK FB, MAHAFFEY EJ, ROBERTS DB, PETERSON MNA (1969) Chemical composition of sediments and interstitial brines from the Atlantis II, Discovery and Chain Deeps. In: DEGENS ET, ROSS DA (eds) *Hot brines and recent heavy metal deposits in the Red Sea*. Springer, New York, pp 407–440
- HENRY DJ, DUTROW BL (2012) Tourmaline at diagenetic to low-grade metamorphic conditions: its petrologic applicability. *Lithos* 154: 16–32
- HENRY DJ, KIRKLAND BL, KIRKLAND DW (1999) Sectorized tourmaline from the cap rock of a salt dome. *Eur J Mineral* 11: 263–280
- HENRY DJ, SUN H, SLACK JF, DUTROW BL (2008) Tourmaline in meta-evaporites and highly magnesian rocks: perspectives from Namibian tourmalinites. *Eur J Mineral* 20: 889–904
- HÖLLER W, GANDHI SM (1997) Origin of tourmaline and oxide minerals from the metamorphosed Rampura Agucha Zn–Pb–(Ag) deposit, Rajasthan, India. *Mineral Petrol* 60: 99–119
- HOUZAR S, NOVÁK M, SELWAY JB (1998) Compositional variation in tourmaline from tourmalinite and quartz segregations at Pernštejn near Nedvědice (Svartka unit, western Moravia, Czech Republic). *J Czech Geol Soc* 43: 53–58
- HÖY T, ANDERSON D, TURNER RJW, LEITCH CHB (2000) Tectonic, magmatic and metallogenic features of the early syn-rift phase of the Purcell Basin, southeastern British Columbia. In: LYDON JW, HÖY T, SLACK JF, KNAPP ME (eds) *Geological environment of the Sullivan deposit, British Columbia*. *Geol Assoc Canada, Min Deposits Div Spec Publ* 1, pp 32–60
- HRISCHEVA E, SCOTT SD (2007) Geochemistry and morphology of metalliferous sediments and oxyhydroxides from the Endeavour segment, Juan de Fuca Ridge. *Geochim Cosmochim Acta* 71: 3476–3497
- HU G, LI Y, FAN C, HOU K, ZHAO Y, ZENG L (2015) In situ LA-MC-ICP-MS boron isotope and zircon U–Pb age determinations of Paleoproterozoic borate deposits in Liaoning Province, northeastern China. *Ore Geol Rev* 65: 1127–1141
- HUMPHRIS SE, TIVEY MK (2000) A synthesis of geological and geochemical investigations of the TAG hydrothermal field: insights into fluid-flow and mixing processes in a hydrothermal system. In: DILEK Y, MOORES E, ELTHON D, NICOLAS A (eds) *Ophiolites and oceanic crust: new insights from field studies and the Ocean Drilling Program*. *Geol Soc Amer Spec Paper* 349, pp 213–235
- HUTTON CO (1939) The significance of tourmaline in the Otago schists. *Royal Soc New Zealand Trans* 68: 599–602

- ITO T, PLIMER IR (1987) The significance of tourmaline in the stratiform Dome Rock deposit, Australia. *Min Geol* 37: 403–418
- JAMTVEIT B, SVENSEN H, PODLADCHIKOV YY, PLANKE S (2004) Hydrothermal vent complexes associated with sill intrusions in sedimentary basins. In: BREITKREUZ C, PETFORD N (eds) *Physical geology of high-level magmatic systems*. Geol Soc London Spec Publ 234, pp 233–241
- JIANG S-Y (1998) Stable and radiogenic isotope studies of tourmaline: an overview. *J Czech Geol Soc* 43: 75–90
- JIANG S-Y (2000) Controls on the mobility of high field strength elements (HFSE), U, and Th in an ancient submarine hydrothermal system of the Proterozoic Sullivan Pb–Zn–Ag deposit, British Columbia, Canada. *Geochem J* 34: 341–348
- JIANG S-Y (2001) Boron isotope geochemistry of hydrothermal ore deposits in China: a preliminary study. *Physics Chem Earth A* 26: 851–858
- JIANG S-Y, PALMER MR, DING T-P, WAN D-F (1994) Silicon isotope geochemistry of the Sullivan Pb–Zn deposit, Canada: a preliminary study. *Econ Geol* 89: 1623–1629
- JIANG S-Y, PALMER MR, LI Y-H, XUE C-J (1995) Chemical compositions of tourmaline in the Qinling Yindongzi-Tongmugou Pb–Zn deposits, China: implications for hydrothermal ore-forming processes. *Miner Depos* 30: 225–234
- JIANG S-Y, PALMER MR, PENG Q-M, YANG J-H (1997) Chemical and stable isotopic compositions of Proterozoic metamorphosed evaporites and associated tourmalines from the Houxianyu borate deposit, eastern Liaoning, China. *Chem Geol* 135: 189–211
- JIANG S-Y, PALMER MR, SLACK JF, SHAW DR (1998) Paragenesis and chemistry of multistage tourmaline formation in the Sullivan Pb–Zn–Ag deposit, British Columbia. *Econ Geol* 93: 47–67
- JIANG S-Y, PALMER MR, SLACK JF, SHAW DR (1999) Boron isotope systematics of tourmaline formation in the Sullivan Pb–Zn–Ag deposit, British Columbia, Canada. *Chem Geol* 158: 131–144
- JIANG S-Y, PALMER MR, SLACK JF, ANDERSON D (2000a) Chemical and boron isotopic composition of tourmaline from massive sulfide deposits and tourmalinites in the Mesoproterozoic Belt and Purcell supergroups, southeastern British Columbia and northwestern Montana. In: LYDON JW, HÖY T, SLACK JF, KNAPP ME (eds) *Geological environment of the Sullivan deposit, British Columbia*. Geol Assoc Canada, Min Deposits Div Spec Publ 1, pp 336–354
- JIANG S-Y, PALMER MR, SLACK JF, DING T-P, WAN D-F (2000b) Silicon isotope compositions of tourmalinites and selected silicate minerals from the Sullivan deposit and vicinity, and their significance to mineral exploration and ore genesis. In: LYDON JW, HÖY T, SLACK JF, KNAPP ME (eds) *Geological environment of the Sullivan deposit, British Columbia*. Geol Assoc Canada, Min Deposits Div Spec Publ 1, pp 782–790
- JIANG S-Y, PALMER MR, SLACK JF, YANG J-H, SHAW DR (2000c) Trace element and rare earth element geochemistry of tourmalinites and related rocks and ores from the Sullivan deposit and vicinity, southeastern British Columbia. In: LYDON JW, HÖY T, SLACK JF, KNAPP ME (eds) *Geological environment of the Sullivan deposit, British Columbia*. Geol Assoc Canada, Min Deposits Div Spec Publ 1, pp 482–495
- JORGE RCGS, RELVAS JMRS, BARRIGA FJAS (2005) Silica gel microtextures in siliceous exhalites at the Soloviejo manganese deposit, Spain. In: MAO J, BIERLEIN FP (eds) *Mineral deposit research: meeting the global challenge*. Proceed 8<sup>th</sup> Bienn SGA Mtg, Beijing. Springer, Berlin, Heidelberg, pp 631–634
- JULIANI C, HACKSPACHER P, DANTAS EL, FETTER AH (2000) The Mesoproterozoic volcano-sedimentary Serra do Itaberaba Group of the central Ribeira belt, São Paulo state, Brazil: implications for the age of the overlying São Roque Group. *Rev Brasil Geoci* 30: 82–86
- KALBSKOPF SP, BARTON JM JR (2003) The Zandvier deposit, Pietersburg green belt, South Africa: an auriferous tourmalinite. *S Afr J Geol* 106: 361–374
- KALLIOMÄKI H, WAGNER T, FUSSWINKEL T, SAKELLARIS G (2017) Major and trace element geochemistry of tourmalines from Archean orogenic gold deposits: proxies for the origin of gold mineralizing fluids? *Ore Geol Rev* 91: 906–927
- KASEMANN S, ERZINGER J, FRANZ G (2000) Boron recycling in the continental crust of the central Andes from the Palaeozoic to Mesozoic, NW Argentina. *Contrib Mineral Petrol* 140: 328–343
- KASTNER M (1982) Evidence for two distinct hydrothermal systems in the Guaymas Basin. In: CURRAY JR, MOORE DG (eds) *Initial Reports, DSDP Leg 64*. U.S. Government Printing Office, Washington, D.C., pp 1143–1157
- KATO A, MATSUBARA S (1980) Manganese borate minerals from Japan. *J Min Soc Japan* 14: 86–97 [in Japanese with English abstract]
- KAWAKAMI T (2001) Tourmaline breakdown in the migmatite zone of the Ryoke metamorphic belt, SW Japan. *J Metamorph Geol* 19: 61–75
- KENNAN PS, KENNEDY MJ (1983) Coticules – a key to correlation along the Appalachian-Caledonian orogen? In: SCHENK PE, HAWORTH RT, KEPPIE JD, TRZCIENSKI WE, WILLIAMS PF, KELLING G (eds) *Regional trends in the geology of the Appalachian-Caledonian-Hercynian-Mauritanide orogen*. Springer, Dordrecht, NATO ASI Series C, 116, pp 355–361
- KISTLER RB, HELVACI C (1994) Boron and borates. In: CARR DD (ed) *Industrial minerals and rocks*, 6<sup>th</sup> Ed. Soc Mining Metall Explor, Littleton, Colorado, pp 171–186
- KLEMMER S, MARSCHALL HR, JACOB DE, PROWATKE S, LUDWIG T (2011) Trace-element partitioning and boron

- isotope fractionation between white mica and tourmaline. *Canad Mineral* 49: 165–176
- KRMÍČEK L, NOVÁK M, TRUMBULL RB, CEMPÍREK J, HOUZAR S (2021) Boron isotopic variations in tourmaline from metacarbonates and associated calc-silicate rocks from the Bohemian massif: constraints on boron recycling in the Variscan orogen. *Geosci Front* 12: 219–230
- LAMBECK A, MERNAGH TP, WYBORN L (2011) Are iron-rich sedimentary rocks the key to the spike in orogenic gold mineralization in the Paleoproterozoic? *Econ Geol* 106: 321–330
- LAURILA TE, HANNINGTON MD, PETERSEN S, GARBE-SCHÖNBERG D (2014) Trace metal distribution in the Atlantis II Deep (Red Sea) sediments. *Chem Geol* 386: 80–100
- LAURILA TE, HANNINGTON MD, LEYBOURNE M, PETERSEN S, DEVEY CW, GARBE-SCHÖNBERG D (2015) New insights into the mineralogy of the Atlantis II Deep metalliferous sediments, Red Sea. *Geochem Geophys Geosys* 16, 4449–4478
- LAWRENCE DM, TRELOAR PJ, RANKIN AH, HARBIDGE P, HOLLIDAY J (2013) The geology and mineralogy of the Loulo mining district, Mali, West Africa: evidence for two distinct styles of orogenic gold mineralization. *Econ Geol* 108: 199–227
- LEAKE RC, FLETCHER CJN, HASLAM HW, KHAN B, SHAKIRULLAH (1989) Origin and tectonic setting of stratabound tungsten mineralization within the Hindu Kush of Pakistan. *J Geol Soc London* 146: 1003–1016
- LEITCH CHB, TURNER RJW (1992) Preliminary field and petrographic studies of the sulfide-bearing network underlying the western orebody, Sullivan stratiform sediment-hosted Zn–Pb deposit, British Columbia. *Geol Survey Canada Curr Res Paper* 92–1E:61–70
- LOTTERMOSER BG (1992) Rare earth elements and hydrothermal ore formation processes. *Ore Geol Rev* 7: 25–41
- LYDON JW (2007) Geology and metallogeny of the Belt–Purcell basin. In: Goodfellow WD (ed) *Mineral deposits of Canada: a synthesis of major deposit-types, district metallogeny, the evolution of geological provinces, and exploration methods*. *Geol Assoc Canada, Min Deposits Div Spec Publ* 5, pp 581–607
- MACGREGOR J, GREW ES, DE HOOG JCM, HARLEY SL, KOWALSKI PM, YATES MG, CARSON CJ (2013) Boron isotopic composition of tourmaline, prismatic, and grandierite from granulite facies paragneisses in the Larsemann Hills, Prydz Bay, East Antarctica: evidence for a non-marine evaporite source. *Geochim Cosmochim Acta* 123: 261–283
- MAHJOUBI EM, CHAUVET A, BADRA L, SIZARET S, BARBANSON L, EL MAZ A, CHEN Y, AMANN M (2016) Structural, mineralogical, and paleoflow velocity constraints on Hercynian tin mineralization: the Achmmach prospect of the Moroccan central massif. *Miner Depos* 51: 431–451
- MANNING CE (2006) Mobilizing aluminum in crustal and mantle fluids. *J Geochem Explor* 89: 251–253
- MAO J (1995) Tourmalinite from northern Guangxi, China. *Miner Depos* 30: 235–245
- MAO J, LI H, LUO Y, WANG C (1995) Tourmalinite from the Liwu massive copper-zinc deposit, west Sichuan, China. In: PAŠAVA J, KŘÍBEK B, ŽÁK K (eds) *Mineral deposits: from their origin to their environmental impacts*. AA Balkema, Rotterdam, *Proceed 3<sup>rd</sup> Ann Bienn SGA Mtg*, Prague, pp 241–244
- MARSCHALL HR (2018) Boron isotopes in the ocean floor realm and the mantle. In: MARSCHALL H, FOSTER G (eds) *Boron isotopes*. Springer, Berlin, *Advances in Isotope Geochemistry* 7, pp 189–215
- MARSCHALL HR, JIANG S-Y (2011) Tourmaline isotopes: no element left behind. *Elements* 7: 313–319
- MARSCHALL HR, KORSAKOV AV, LUVIZOTTO GL, NASDALA L, LUDWIG T (2009) On the occurrence and boron isotopic composition of tourmaline in (ultra)high-pressure metamorphic rocks. *J Geol Soc London* 166: 811–823
- MARSCHALL HR, WANLESS VD, SHIMIZU N, POGGE VON STRANDMANN PAE, ELLIOTT T, MONTELEONE BD (2017) The boron and lithium isotopic composition of mid-ocean ridge basalts and the mantle. *Geochim Cosmochim Acta* 207: 102–138
- MARTIN W, BAROSS J, KELLEY D, RUSSELL MJ (2008) Hydrothermal vents and the origin of life. *Nat Rev Microbiol* 6: 805–814
- MARTÍNEZ-MARTÍNEZ JM, TORRES-RUIZ J, PESQUERA A, GIL-CRESPO PP (2010) Geological relationships and U–Pb zircon and <sup>40</sup>Ar/<sup>39</sup>Ar tourmaline geochronology of gneisses and tourmalinites from the Nevado-Filabride complex (western Sierra Nevada, Spain): tectonic implications. *Lithos* 119: 238–250
- MCARDLE P, KENNAN PS (1992) Deformational and stratigraphic influences on mineralization in SE Ireland. *Miner Depos* 27: 213–218
- MCARDLE P, FITZELL M, OOSTEROM MG, O’CONNOR PJ, KENNAN PS (1989) Tourmalinite as a potential host rock for gold in the Caledonides of southeast Ireland. *Miner Depos* 24:154–159
- MCGLOIN MV (2017) The significance of metaexhalites, seafloor alteration and retrograde processes for metamorphosed mineral deposits: examples of distinct alteration styles from the Aileron Province. *Proceed Northern Territory Geol Surv Ann Geosci Expl Seminar*, Darwin, pp 42–50
- MCGLOIN M, MAAS R, WEISHEIT A, MEFFRE S, THOMPSON J, ZHUKOVA I, STEWART J, HUTCHINSON G, TRUMBULL R, CREASER R (2016) Palaeoproterozoic copper mineralisation in the Aileron Province: new findings on temporal, spatial and genetic features. *Proceed Northern Territory Geol Surv Ann Geosci Expl Seminar*, Darwin, pp 63–74

- MCGLOIN MV, WEISHEIT A, TRUMBULL RB, MAAS R (2019) Using tourmaline to identify base metal and tungsten mineralising processes in the Jervois mineral field and Bonya Hills, Aileron Province. Northern Territory Geol Survey Rec 2019–001, 46 p
- MICHAILIDIS K, KASSOLI-FOURNARAKIA (1994) Tourmaline concentrations in migmatitic metasedimentary rocks of the Riziana and Kolchiko areas in Macedonia, northern Greece. *Eur J Mineral* 6: 557–569
- MILTON C (1971) Authigenic minerals of the Green River Formation. *Wyoming Univ Contrib Geol* 10: 57–63
- MISHIMA S, OHTOMO Y, KAKEGAWA T (2016) Occurrence of tourmaline in metasedimentary rocks of the Isua supracrustal belt, Greenland: implications for ribose stabilization in Hadean marine sediments. *Origins Life Evol Biosph* 46: 247–271
- MITICH GB (1946) A tourmaline-bearing horizon in the quartzites of the Aldan plate. *Dokl Akad Nauk Leningrad* 53: 243–245
- MITTWEDE SK (1984) Tourmalinite, anomalous tourmaline concentrations, and iron formation as exploration guides in northwestern Cherokee County, South Carolina. *South Carolina Geol* 27: 6–12
- MITTWEDE SK (1990) The central Piedmont metallogenic province, South Carolina. In: COOK RB (ed) *Proceed Symp Econ Min Deposits Southeast: metallic ore deposits*. Georgia Geol Survey Bull 117, pp 177–207
- MITTWEDE SK, HELVACI C, KARAMANDERESI İH, KUN N, CANDAN O (1992) Modes and implications of tourmaline occurrences in the Menderes massif, western Anatolia, Türkiye. In: ANIL M, NAZIK A (eds) *Proceed Inter Symp Eastern Mediterranean Geol, Adana*. Geosound 20, pp 179–190
- MODRESKI PJ, CONNOR JJ (1991) Tourmalinites and iron formation in the Yellowjacket Formation, Idaho cobalt belt, Lemhi County, Idaho. *US Geol Survey Circ* 1062, 57 p
- NABELEK PI (2021) Formation of metasomatic tourmalinites in reduced schists during the Black Hills orogeny, South Dakota. *Amer Miner* 106: 282–289
- NANTEL S (1994a) Association coticules-tourmalinites et minéralisations en  $Cu \pm Co \pm Au$  dans la région de Saint-Jovite, partie sud de la Province de Grenville: importance de ce métallotecte pour l'exploration de gîtes de type exhalative. *Québec Minist Res Natur Rapp MB* 94–15, 16 p
- NANTEL S (1994b) Les tourmalinites et les roches riches en tourmaline dans la partie sud de la Province de Grenville, Québec, et leur association avec des minéralisations en Zn et en  $Cu-Co \pm Au$ . *Québec Minist Res Natur Rapp MB* 94–52, 24 p
- NDIAYE PM, GUILLOU JJ (1997) Les tourmalinites stratiformes à dravite d'origine colloïdale du Paléoproterozoïque sénégal-malien. *J Afr Earth Sci* 24: 215–226
- NESBITT BE, LONGSTAFFE FJ, SHAW DR, MUEHLENBACHS K (1984) Oxygen isotope geochemistry of the Sullivan massive sulfide deposit, Kimberley, British Columbia. *Econ Geol* 79:933–946
- NEVEU M, KIM HJ, BENNER SA (2013) The “strong” RNA world hypothesis: fifty years old. *Astrobiol* 13: 391–403
- NICHOLSON PM (1980) The geology and economic significance of the Golden Dyke dome, Northern Territory. In: FERGUSON J, GOLEBY AB (eds) *Uranium in the Pine Creek geosyncline*. Inter Atomic Energy Agency, Vienna, pp 319–334
- NIE F-J (1993) Genesis of the Bieluwutu volcanogenic copper deposit, south-central Inner Mongolia, People's Republic of China. *Inter Geol Rev* 35: 805–824
- NIE FJ, ZHANG HT, SUN H, FAN JT (1990) Discovery of tourmalinites in the Bieluwutu copper metallogenic district, Nei Mongol and their geological significance. *Geol Rev* 36: 467–472 [in Chinese with English abstract]
- NIINISKORPI V (1986) Stratabound tourmaline-rich rocks in Kurkkionvaara area, northern Sweden. *Proceed Seventh Quad IAGO Symp, Luleå, Sweden*, poster session abstract
- OEHLER JH (1976) Hydrothermal crystallization of silica gel. *Geol Soc Am Bull* 87: 1143–1152
- OTA T, AIHARA Y, KIYOKAWA S, TANAKA R, NAKAMURA E (2019) Tourmaline in a Mesoarchean pelagic hydrothermal system: implications for the habitat of early life. *Precamb Res* 334, doi 10.1016/j.precamres.2019.105475
- PALMER MR (1991) Boron isotope systematics of hydrothermal fluids and tourmalines: a synthesis. *Chem Geol* 94: 111–121
- PALMER MR, SLACK JF (1989) Boron isotopic composition of tourmaline from massive sulfide deposits and tourmalinites. *Contrib Mineral Petrol* 103: 434–451
- PAVLIDES L, GAIR JE, CRANFORD SL (1982) Central Virginia volcanic-plutonic belt as a host for massive sulfide deposits. *Econ Geol* 77: 233–272
- PENG QM, PALMER MR (1995) The Palaeoproterozoic boron deposits in eastern Liaoning, China: a metamorphosed evaporite. *Precamb Res* 72: 185–197
- PENG Q-M, PALMER MR (2002) The Paleoproterozoic Mg and Mg–Fe borate deposits of Liaoning and Jilin provinces, northeast China. *Econ Geol* 97: 93–108
- PERTOLD Z, CHRT J, BUDIL V, BURDA J, BURDOVÁ P, KŘÍBEK B, PERTOLDOVÁ J GASKARTH B (1994) The Tisová Cu deposit: a Besshi-type mineralization in the Krušné hory Mts., Bohemian Massif, Czech Republic. In: VON GEHLEN K, KLEMM DD (eds) *Mineral deposits of the Erzgebirge/Krušné hory (Germany/Czech Republic)*. E. Schweizerbart'sche Verlagsbuchhandlung, Stuttgart, Mono Series Min Deposits 31, pp 71–95
- PESQUERA A, VELASCO F (1997) Mineralogy, geochemistry and geological significance of tourmaline-rich rocks from the Paleozoic Ceinco Villas massif (western Pyrenees, Spain). *Contrib Mineral Petrol* 129: 53–74

- PESQUERA A, TORRES-RUIZ J, GIL-CRESPO PP, JIANG S-Y (2005) Petrographic, chemical and B-isotopic insights into the origin of tourmaline-rich rocks and boron recycling in the Martinamor antiform (central Iberian zone, Salamanca, Spain). *J Petrol* 46: 1013–1044
- PESQUERA A, TORRES-RUIZ J, GIL-CRESPO PP, RODA-ROBLES E (2009) Multistage boron metasomatism in the Alamo Complex (central Iberian Zone, Spain): evidence from field relations, petrography, and  $^{40}\text{Ar}/^{39}\text{Ar}$  tourmaline dating. *Amer Miner* 94: 1468–1478
- PESQUERA A, GIL-CRESPO PP, TORRES-RUIZ J, RODA-ROBLES E (2018) Insights into petrogenesis of the Jálama pluton (central Iberian zone, western Spain). *Int Geol Rev* 60: 157–187
- PETERSEN JS, KOED JO, SUNDBLAD K (1995) Stratiform, sediment-hosted Zn–Pb mineralization at Espeland in the Proterozoic Bamble shear belt, southern Norway. In: PAŠAVA J, KRÍBEK B, ŽÁK K (eds) *Mineral deposits: from their origin to their environmental impacts*. Proceed 3<sup>rd</sup> Bienn SGA Mtg, Prague, AA Balkema, Rotterdam, pp 307–310
- PIRAJNO F (2013) Effects of metasomatism on mineral systems and their host rocks: alkali metasomatism, skarns, greisens, tourmalinites, rodingites, black-wall alteration and listvenites. In: HARLOV DE, AUSTRHEIM H (eds) *Metasomatism and the chemical transformation of rock*. Springer-Verlag, Berlin-Heidelberg, pp 203–251
- PLIMER IR (1986) Tourmalinites from the Golden Dyke dome, northern Australia. *Miner Depos* 21: 263–270
- PLIMER IR (1987) The association of tourmalinite with stratiform scheelite deposits. *Miner Depos* 22: 282–291
- PLIMER IR (1988) Tourmalinites associated with Australian Proterozoic submarine exhalative ores. In: FRIEDRICH GH, HERZIG PM (eds) *Base metal sulfide deposits*. Springer, Berlin, pp 255–283
- RAITH JG (1988) Tourmaline rocks associated with stratabound scheelite mineralisation in the Austroalpine crystalline complex, Austria. *Miner Petrol* 39: 265–288
- RAITH JG, RIEMER N, MEISEL T (2004) Boron metasomatism and behavior of rare earth elements during formation of tourmaline rocks in the eastern Arunta Inlier, central Australia. *Contrib Mineral Petrol* 147: 91–109
- RAVEGGI M, GILES D, FODEN J, RAETZ M, EHLERS K (2008) Source and significance of the felsic magmatism in the Paleoproterozoic to Mesoproterozoic Broken Hill block, New South Wales. *Aust J Earth Sci* 55: 531–553
- REINECKE T, OKRUSCH M, RICHTER P (1985) Geochemistry of ferromanganoan metasediments from the island of Andros, Cycladic blueschist belt, Greece. *Chem Geol* 53: 249–278
- REYNOLDS RD JR (1965) Geochemical behaviour of boron during the metamorphism of carbonate rocks. *Geochim Cosmochim Acta* 29: 1101–1114
- RIEHL W, CABRAL AR (2018) Meta-evaporite in the Carajás mineral province, northern Brazil. *Miner Depos* 53: 895–902
- ROMER RL, MEIXNER A, HAHNE K (2014) Lithium and boron isotopic composition of sedimentary rocks – the role of source history and depositional environment: a 250 Ma record from the Cadomian orogeny to the Variscan orogeny. *Gondwana Res* 26: 1093–1110
- SANGSTER D (2002) The role of dense brines in the formation of vent-distal sedimentary-exhalative (SEDEX) lead–zinc deposits: field and laboratory evidence. *Miner Depos* 37: 149–157
- SCHIRA W, AMSTUTZ GC, FONTBOTÉ L (1990) The Piren Alto Cu–(Zn) massive sulfide occurrence in south-central Chile – a Kieslager-type mineralization in a Paleozoic ensialic mature marginal basin setting. In: FONTBOTÉ L, AMSTUTZ GC, CARDOZO M, CEDILLO E, FRUTOS J (eds) *Stratabound ore deposits in the Andes*. Springer-Verlag, Berlin-Heidelberg, pp 229–251
- SCHMIDT M, AL-FARAWATI R, BOTZ R (2015) Geochemical classification of brine-filled Red Sea deeps. In: RASUL NMA, STEWART ICF (eds) *The Red Sea*. Springer-Verlag, Berlin-Heidelberg, pp 219–233
- SEAL RR II, SLACK JF, SHAW DR (2000) Oxygen and hydrogen isotope systematics of tourmalinites and associated rocks from the Sullivan mine, B.C, and elsewhere in the Belt-Purcell Supergroup. In: LYDON JW, HÖY T, SLACK JF, KNAPP ME (eds) *Geological environment of the Sullivan deposit, British Columbia*. Geol Assoc Canada, *Min Deposits Div Spec Publ* 1, pp 768–781
- SENGUPTA N, MUKHOPADHYAY D, SENGUPTA P, HOFFBAUER R (2005) Tourmaline-bearing rocks in the Singhbhum shear zone, eastern India: evidence of boron infiltration during regional metamorphism. *Amer Miner* 90: 1241–1255
- SLACK JF (1980) Tourmaline – a prospecting guide for massive base-metal sulfide deposits in the Penobscot Bay area, Maine. *Maine Geol Survey Spec Econ Studies Ser* 8, 25 p
- SLACK JF (1982) Tourmaline in Appalachian–Caledonian massive sulfide deposits and its exploration significance. *Inst Mining Metall Trans* 91: B81–B89
- SLACK JF (1993) Models for tourmalinite formation in the Middle Proterozoic Belt and Purcell supergroups (Rocky Mountains) and their exploration significance. *Geol Survey Canada, Current Res Paper* 93–1E: 33–40
- SLACK JF (1996) Tourmaline associations with hydrothermal ore deposits. In: GREW ES, ANOVITZ LM (eds) *Boron: mineralogy, petrology and geochemistry*. *Rev Mineral* 33, pp 559–643 [Updated version published as 2<sup>nd</sup> Edition in 2002]
- SLACK JF (2020) Potential for Sullivan-type Pb–Zn–Ag deposits in modern marine basins. *Miner Depos* 55: 1271–1278

- SLACK JF, HÖY T (2000) Geochemistry and provenance of clastic metasedimentary rocks of the Aldridge and Fort Steele formations, Purcell Supergroup, southeastern British Columbia. In: LYDON JW, HÖY T, SLACK JF, KNAPP ME (eds) Geological environment of the Sullivan deposit, British Columbia. Geol Assoc Canada, Min Deposits Div Spec Publ 1, pp 180–201
- SLACK JF, ROBINSON GR JR (1990) Retrograde metamorphic breakdown of tourmaline at Broken Hill, Australia. Geol Soc Amer Abs Pgms 22(7): 126
- SLACK JF, STEVENS BPJ (1994) Clastic metasediments of the Early Proterozoic Broken Hill Group, New South Wales, Australia: geochemistry, provenance, and metallogenic significance. Geochim Cosmochim Acta 58: 3633–3652
- SLACK JF, TRUMBULL RB (2011) Tourmaline as a recorder of ore-forming processes. Elements 7: 321–326
- SLACK JF, HERRIMAN N, BARNES RG, PLIMER IR (1984) Stratiform tourmalinites in metamorphic terranes and their geologic significance. Geology 12: 713–716
- SLACK JF, PALMER MR, STEVENS BP (1989) Boron isotope evidence for the involvement of non-marine evaporites in the origin of the Broken Hill ore deposits. Nature 342: 913–916
- SLACK JF, PALMER MR, STEVENS BPJ, BARNES RG (1993) Origin and significance of tourmaline-rich rocks in the Broken Hill district, Australia. Econ Geol 88: 505–541
- SLACK JF, PASSCHIER CW, ZHANG JS (1996) Metasomatic tourmalinite formation along basement-cover décollements, Orobic Alps, Italy. Schweiz Min Pet Mitt 76: 193–207
- SLACK JF, MCGEE JJ, GRIFFIN WL, WIN TT, RYAN CG (1997) Geochemistry and origin of complexly zoned tourmaline crystals in the Ore Knob massive sulfide deposit, North Carolina, U.S.A. In: NOVÁK M (ed) Tourmaline 1997 Conference. Moravian Museum, Brno, Czech Republic, Abstracts and Program, pp 97–98
- SLACK JF, TURNER RJW, WARE PLG (1998) Boron-rich mud volcanoes of the Black Sea region: modern analogues to ancient sea-floor tourmalinites associated with Sullivan-type Pb–Zn deposits? Geology 26: 439–442
- SLACK JF, MEIER AL, MALCOLM MJ, FEY DL, DOUGHTEN MW, WANDLESS GA (2000a) Trace element and rare-earth element geochemistry of bedded and massive sulfides from the Sullivan Pb–Zn–Ag deposit, British Columbia – a reconnaissance study. In: LYDON JW, HÖY T, SLACK JF, KNAPP ME (eds) Geological environment of the Sullivan deposit, British Columbia. Geol Assoc Canada, Min Deposits Div Spec Publ 1, pp 720–735
- SLACK JF, SHAW DR, LEITCH CHB, TURNER RJW (2000b) Tourmalinites and cotiules from the Sullivan Pb–Zn–Ag deposit and vicinity, British Columbia: geology, geochemistry, and genesis. In: LYDON JW, HÖY T, SLACK JF, KNAPP ME (eds) Geological environment of the Sullivan deposit, British Columbia. Geol Assoc Canada, Min Deposits Div Spec Publ 1, pp 736–767
- SLACK JF, OFFIELD TW, WOODRUFF LG, SHANKS WC III (2001) Geology and geochemistry of Besshi-type massive sulfide deposits of the Vermont copper belt. Soc Econ Geol Guidebook Ser 35: 193–211
- SLACK JF, NEYMARK LA, MOSCATI RJ, LOWERS HA, RANSOM PW, HAUSER RL, ADAMS DT (2020) Origin of tin mineralization in the Sullivan Pb–Zn–Ag deposit, British Columbia: constraints from textures, geochemistry, and LA-ICP-MS U–Pb geochronology of cassiterite. Econ Geol 115: 1699–1724
- SPIVACK AJ, PALMER MR, EDMOND JM (1987) The sedimentary cycle of the boron isotopes. Geochim Cosmochim Acta 51: 1939–1949
- SPRÁNITZ T, JÓZSA S, KOVÁCS Z, VÁCZI B, TÖRÖK K (2018) Magmatic and metamorphic evolution of tourmaline-rich rocks of the Sopron area, eastern Alps (W. Hungary). J Geosci 63: 175–191
- SPRY PG (1990) Geochemistry and origin of cotiules (spessartine-quartz rocks) associated with metamorphosed massive sulfide deposits. In: SPRY PG, BRYNDZIA LT (eds) Regional metamorphism of ore deposits and genetic implications. VSP Publishers, Utrecht, pp 49–75
- SPRY PG, TEALE GS (2021) A classification of Broken Hill-type deposits: a critical review. Ore Geol Rev 130, <https://doi.org/10.1016/j.oregeorev.2020.103935>
- SPRY PG, PETER JM, SLACK JF (2000) Meta-exhalites as exploration guides to ore. Rev Econ Geol 11: 163–201
- STEVEN NM, MOORE JM (1995) Tourmalinite mineralization in the Late Proterozoic Kuiseb Formation of the Damara orogen, central Namibia: evidence for a replacement origin. Econ Geol 90: 1098–1117
- STEVENS BPJ, BRADLEY GM (2018) Sedimentology in metamorphic rocks, the Willyama Supergroup, Broken Hill, Australia. Aust J Earth Sci 65: 25–59
- SU Z-K, ZHAO X-F, LI X-C, ZHOU M-F (2016) Using elemental and boron isotopic compositions of tourmaline to trace fluid evolutions of IOCG systems: the worldclass Dahongshan Fe–Cu deposit in SW China. Chem Geol 441: 265–279
- SUN H-T, GE CH (1989) Discovery of banded tourmalinite and mineralized tourmaline-rich chemical sedimentary rocks from stratabound and stratiform copper deposits in Zhongtiaoshan district, Shanxi province. Chinese Sci Bull 34: 846–851
- TAYLOR BE, SLACK JF (1984) Tourmalines from Appalachian–Caledonian massive sulfide deposits: textural, chemical, and isotopic relationships. Econ Geol 79: 1703–1726
- TAYLOR BE, TURNER RJW, LEITCH CHB, WATANABE DH, SHAW DR (2000) Oxygen and hydrogen isotope evidence for the origins of mineralizing and alteration fluids, Sullivan Pb–Zn mine and vicinity, British Columbia. In: LYDON JW, HÖY T, SLACK JF, KNAPP ME (eds) Geological environment of the Sullivan deposit, British

- Columbia. Geol Assoc Canada, Min Deposits Div Spec Publ 1, pp 652–672
- THEART HFJ, CORNELL DH, SCHADE J (1989) Geochemistry and metamorphism of the Prieska Zn–Cu deposit, South Africa. *Econ Geol* 84: 34–48
- TORRES-RUIZ J, PESQUERA A, GIL-CRESPO PP, VELILLA N (2003) Origin and petrogenetic implications of tourmaline-rich rocks in the Sierra Nevada (Betic Cordillera, southeastern Spain). *Chem Geol* 197: 55–86
- TOURN SM, HERRMANN CJ, AMETRANO S, DE BRODTKORB MK (2004) Tourmalinites from the eastern Sierras Pampeanas, Argentina. *Ore Geol Rev* 24: 229–240
- TRUMBULL RB, SLACK JF (2018) Boron isotopes in the continental crust: granites, pegmatites, felsic volcanic rocks, and related ore deposits. In: MARSCHALL HR, FOSTER GL (eds) Boron isotopes – the fifth element. Springer-Verlag, Berlin-Heidelberg, *Advances in Isotope Geochemistry* 7, pp 249–272
- TRUMBULL RB, KRIENITZ M-S, GOTTESMANN B, WIEDENBECK M (2008) Chemical and boron-isotope variations in tourmalines from an S-type granite and its source rocks: the Erongo granite and tourmalinites in the Damara Belt, Namibia. *Contrib Mineral Petrol* 155: 1–18
- TRUMBULL RB, SLACK JF, KRIENITZ M-S, BELKIN HE, WIEDENBECK M (2011) Fluid sources and metallogenesis in the Blackbird Co–Cu–Au–Bi–Y–REE district, Idaho, U.S.A.: insights from major-element and boron isotopic compositions of tourmaline. *Canad Mineral* 49: 225–244
- TRUMBULL RB, GARDA GM, XAVIER RP, CAVALCANTI JAD, CODEÇO MS (2019) Tourmaline in the Passagem de Mariana gold deposit (Brazil) revisited: major-element, trace-element and B-isotope constraints on metallogenesis. *Miner Depos* 54: 395–414
- TRUMBULL RB, CODEÇO MS, JIANG S-Y, PALMER MR, SLACK JF (2020) Boron isotope variations in tourmaline from hydrothermal ore deposits: a review of controlling factors and insights for mineralizing systems. *Ore Geol Rev* 125, doi 10.1016/j.oregeorev.2020.103682
- TURNER RJW, LEITCH CHB, HÖY T, RANSOM PW, HAGEN A, DELANEY GD (2000) Sullivan graben system: district-scale setting of the Sullivan deposit. In: LYDON JW, HÖY T, SLACK JF, KNAPP ME (eds) Geological environment of the Sullivan deposit, British Columbia. Geol Assoc Canada, Min Deposits Div Spec Publ 1, pp 370–407
- VAN HINSBERG VJ, HENRY DJ, MARSCHALL HR (2011) Tourmaline: an ideal indicator of its host environment. *Canad Mineral* 49: 1–16
- VAN HINSBERG VJ, SCHUMACHER JC, SLACK JF, MARSCHALL H (2017) Trace elements in tourmaline. Tourmaline 2017 Conference, Skalsky Dvur, Czech Republic, June 23–28, 2017, Abstracts Volume, pp 94–95
- VAN KRANENDONK MJ, BAUMGARTNER R, DJOKIC T, OTA T, STELLER L, GARBE U, NAKAMURA E (2021) Elements for the origin of life on land: a deep-time perspective from the Pilbara Craton of Western Australia. *Astrobiol* 21: 39–59
- VIAL DS, DUARTE BP, FUZIKAWA K, VIEIRA MBH (2007) An epigenetic origin for the Passagem de Mariana gold deposit, Quadrilátero Ferrífero, Minas Gerais, Brazil. *Ore Geol Rev* 32: 596–613
- VISHWAKARMA RK (1996) 1.66-Ga-old metamorphosed Pb–Cu deposit in Sargipali (eastern India): manifestations of tidal flat environment and sedex-type genesis. *Precambr Res* 77: 117–130
- WAGENER JHF, VAN SCHALKWYK L (1986) The Prieska zinc-copper deposit, northern Cape Province. In: ANHAEUSSER CR, MASKE S (eds) Mineral deposits of southern Africa. Geol Soc South Africa, Johannesburg, 2, pp 1503–1529
- WARR LN (2021) IMA-CNMNC approved mineral symbols. *Mineral Mag* 85:291–320
- WEISS MC, SOUSA FL, MRNJAVAC N, NEUKIRCHEN S, ROETTGER M, NELSON-SATHI S, MARTIN WF (2016) The physiology and habitat of the last universal common ancestor. *Nature Microbiol*: 1.9: 1–8
- WILLNER AP (1992) Tourmalinites from the stratiform peraluminous metamorphic suite of the central Namaqua mobile belt (South Africa). *Miner Depos* 27: 304–313
- XU H, PENG Q-M, PALMER MR (2004) Origin of tourmaline-rich rocks in a Paleoproterozoic terrane (N.E. China): evidence for evaporite-derived boron. *Geology China* 31: 240–253
- YAMAOKA K, HONG E, ISHIKAWA T, GAMO T, KAWAHATA H (2015) Boron isotope geochemistry of vent fluids from arc/back-arc seafloor hydrothermal systems in the western Pacific. *Chem Geol* 392: 9–18
- YAN X-L, CHEN B (2014) Chemical and boron isotopic compositions of tourmaline from the Paleoproterozoic Houxianyu borate deposit, NE China: implications for the origin of borate deposit. *J Asian Earth Sci* 94: 252–266
- YANG S-Y, JIANG S-Y (2012) Chemical and boron isotopic composition of tourmaline in the Xiangshan volcanic-intrusive complex, southeast China: evidence for boron mobilization and infiltration during magmatic-hydrothermal processes. *Chem Geol* 312–313: 177–189
- YARDLEY BWD (2013) The chemical composition of metasomatic fluids in the crust. In: HARLOV DE, AUSTRHEIM H (eds) Metasomatism and the chemical transformation of rock. Springer-Verlag, Berlin-Heidelberg, pp 17–52
- YÜCEL-ÖZTÜRK Y, HELVACI C, PALMER MR, ERSOY Y, FRESLON N (2015) Origin and significance of tourmalinites and tourmaline-bearing rocks of Menderes massif, western Anatolia, Turkey. *Lithos* 218–219: 22–36
- ZANCHI A, ZANCHETTA S, BERIO L, BERRA F, FELLETTI F (2019) Low-angle normal faults record Early Permian extensional tectonics in the Orobic Basin (southern Alps, N Italy). *Italian J Geosci* 138: 184–201
- ZHAO F, BERNDT C, ALVES TM, XIA S, LI L, MI L, FAN C (2021) Widespread hydrothermal vents and associ-

- ated volcanism record prolonged Cenozoic magmatism in the South China Sea. *Geol Soc Am Bull* 133: 2645–2660
- ZHONG R, BRUGGER J, CHEN Y, LI W (2015) Contrasting regimes of Cu, Zn and Pb transport in ore-forming hydrothermal fluids. *Chem Geol* 395: 154–164
- ZIERENBERG RA, SHANKS WC III (1983) Mineralogy and geochemistry of epigenetic features in metalliferous sediment, Atlantis II Deep, Red Sea. *Econ Geol* 78: 57–72
- ZIERENBERG RA, SHANKS WC III (1988) Isotopic studies of epigenetic features in metalliferous sediment, Atlantis II Deep, Red Sea. *Canad Mineral* 26: 737–753